Quaternary Science Reviews 296 (2022) 107804

Contents lists available at ScienceDirect

Quaternary Science Reviews

journal homepage: www.elsevier.com/locate/quascirev

Eurasian Ice Sheet derived meltwater pulses and their role in driving atmospheric dust activity: Late Quaternary loess sources in SE England

Yunus Baykal [a, *], Thomas Stevens [a], Mark D. Bateman [b], Katharina Pfaff [c], Daniele Sechi [d], Adriano Banak [e], Sanja Šuica [f], Haobo Zhang [g], Junsheng Nie [g]

[a] Department of Earth Sciences, Uppsala University, Uppsala, Sweden
[b] Department of Geography, University of Sheffield, Sheffield, UK
[c] Department of Geology and Geological Engineering, Colorado School of Mines, Golden, USA
[d] Department of Architecture, Design and Planning, University of Sassari, Alghero, Italy
[e] Department of Geology, Croatian Geological Survey, Zagreb, Croatia
[f] INA-Industrija nafte, d.d., Exploration and Production Laboratory, Croatia
[g] Key Laboratory of Western China's Environmental Systems (Ministry of Education), College of Earth and Environmental Sciences, Lanzhou University, Lanzhou, China

ARTICLE INFO

Article history:
Received 31 July 2022
Received in revised form
20 September 2022
Accepted 27 September 2022
Available online xxx

Handling Editor: Dr C. O'Cofaigh

Keywords:
Provenance
Detrital zircon U–Pb ages
Heavy minerals
Nd isotopes
Quartz grain morphology
Pegwell Bay

ABSTRACT

The role of Quaternary ice sheet fluctuations in driving meltwater pulses and ocean circulation perturbations is widely acknowledged. What is less clear is the role of these processes in driving changes in past atmospheric dust activity, and possible wider links between dust and climate. Terrestrial windblown dust (loess) deposits along the northern fringe of the European loess belt potentially record past atmospheric dust emission from regions close to the former Eurasian Ice Sheet (EIS) and provide a means to evaluate the role of ice sheet fluctuations in the past dust cycle. Numerical loess chronologies across this region generally agree on greatly enhanced dust deposition rates during MIS 2, when the EIS reached its maximum extent. Yet, uncertainties over the sources of this material prevent understanding of the precise causes of this greatly enhanced atmospheric dustiness, and any potential link to ice sheet fluctuations and climate. In southeast England, loess accumulation dominantly occurred in two phases centered on 25–23.5 ka and 20–19 ka, matching the timing of coalescence of the Fennoscandian and British-Irish ice sheets and specifically advances and retreats of nearby ice lobes in the western North Sea. As such, these deposits provide an ideal test of the role of ice sheet fluctuations in atmospheric dust dynamics. Here we undertake such a test through a detailed provenance study of loess in southeast England and potential dust source sediments across the North Sea region. We group extensive new and published data sets of detrital zircon U–Pb ages from basement rocks and Cenozoic sediments in the North Sea area, which not only provide new insight into both loess source, but also the nature of sediment transport over NW Europe into the North Sea basin more widely. Multi-proxy evidence allows us to unambiguously identify ice sheet derived sediments in the exposed North Sea basin as the dominant source of loess in southeast England, while fluvial sediments delivered by rivers draining Continental Europe possibly contributed additional source material to the first loess accumulation phase. We propose that sudden retreats of the North Sea Lobe released substantial amounts of sediment rich meltwater into the southern North Sea and Channel basins, driving accelerated dust emission, loess deposition and provenance variability in NW Europe during MIS 2. Moreover, we propose that this model of dust activity driven by proglacial sediment availability may be applicable for EIS marginal regions more widely, even where resultant loess cover is rarely preserved due to extensive erosion and reworking along the ice marginal spillway. This implies the role of ice sheets in controlling wider dust emission may be underestimated. In addition to driving changes in ocean circulation through meltwater pulses, ice sheet dynamics in the Quaternary may have also driven substantial and abrupt changes in atmospheric dust activity. This mechanism may in part explain the coupling between dust and climate

* Corresponding author.
E-mail address: yunus.baykal@geo.uu.se (Y. Baykal).

https://doi.org/10.1016/j.quascirev.2022.107804

events widely seen in Quaternary dust sediment records and suggests a possible major role of high latitude dust emission in MIS 2 dustiness across Europe and beyond.

1. Introduction

The role of ice sheets in driving meltwater pulses that in turn affect ocean circulation and climate during the Quaternary is widely acknowledged (Ruddiman et al., 1980; Rahmstorf, 2002; Denton et al., 2010). Deglaciation of the last Eurasian Ice Sheet (EIS) was characterized by phases of sudden, rapid ice margin retreat (Toucanne et al., 2015; Sejrup et al., 2016; Roberts et al., 2018; Brendryen et al., 2020). These events led to multiple environmental consequences, including meltwater-driven perturbations in circulation of the North Atlantic Ocean which, in turn, potentially caused large scale, abrupt climate reorganizations (Toucanne et al., 2015, 2021). Along with ice sheet-derived meltwater, large volumes of sediment were also released into ice-marginal regions, dramatically reshaping proglacial landscapes (Weckwerth et al., 2019) and providing excellent sources for aeolian dust deflation (Schaffernicht et al., 2020). Atmospheric mineral dust interacts with climate through multiple feedbacks involving nutrient cycling, albedo and radiative forcing (Knippertz, 2014; Bullard et al., 2016), and numerous studies on Quaternary dust deposits show close associations of abrupt dust deposition variability with abrupt climate change (Stevens et al., 2008; Rasmussen et al., 2014; Újvári et al., 2017). Furthermore, recent research suggests that relatively ice-marginal regions in Europe cannot be ruled out as potential sources for last glacial dust over Greenland (Újvári et al., 2022), leaving open the possibility that ice sheet driven dust events may have hemispheric-scale effects. Indeed, the importance of modern high latitude dust more generally has been underestimated (Bullard et al., 2016; Meinander et al., 2022). However, the impact of ice sheet events on dust emission, abrupt climate change, loess deposition and the wider landscape remains unclear.

Past changes in dust emission from areas proximal to former ice sheets are potentially recorded in loess deposits along the northern fringe of the European loess belt (Antoine et al., 2003; Lehmkuhl et al., 2016; Stevens et al., 2020; Baykal et al., 2021). These loess deposits are especially good records of "coarse dust" ($\geq$5 μm), the specific forcing effects of which tend to be underestimated in climate models (Adebiyi and Kok, 2020). Loess chronologies across this region suggest that especially thick deposits were emplaced during MIS 2 (29–14 ka) when the EIS was at its most dynamic (Guérin et al., 2017; Moine et al., 2017; Zens et al., 2017; Moska et al., 2019). However, uncertainties over the sources of this material and the mechanisms involved during dust particle production limit understanding of the causes of this greatly enhanced atmospheric dustiness during MIS 2, and have prevented any testing of links between fluctuations in dust deposition and ice sheet dynamics. Traditionally, loess deposits along the northern fringe of the European loess belt have been suggested to be sourced from northern ice sheet derived material (Smalley and Leach, 1978). Under this model, seasonal glacial melt releases large amounts of sediment-laden meltwater causing formation of extensive glaciofluvial outwash plains (Vandenberghe and Woo, 2002) that in turn act as a ready source for aeolian dust deflation and loess deposition. This sediment availability in proglacial systems was dramatically increased during ice sheet recession phases accompanied by catastrophic outburst floods along the EIS margin (Marren, 2002; Roberts et al., 2018; Weckwerth et al., 2019). Based on this concept for dust particle production, sediment supply to former ice marginal regions in Northern Europe would have been substantially increased during the Last Glacial Maximum (LGM) and subsequent early deglaciation, potentially accounting for concurrent enhanced atmospheric dustiness recorded in the region's loess deposits. Furthermore, abrupt, coupled ice sheet-climate events, such as Heinrich events, have also been shown to coincide with enhanced dust deposition in both source proximal loess deposits (Stevens et al., 2011; Moine et al., 2017; Újvári et al., 2017) and on source distal ice sheets such as Greenland (Fuhrer et al., 1999). However, the mechanism for this coupling remains unclear, and the relative importance of dust and climate changes in driving these coupled events is poorly constrained.

More fundamentally, the role of ice sheets in producing sufficient material to generate loess deposits in Europe and atmospheric dust loading more widely is debated (Smalley et al., 2009; Újvári et al., 2015; Baykal et al., 2021; Bunce et al., 2022). In particular, provenance study of last glacial loess and other sediments in the Northern European Plain identified a mixture of Fennoscandian Ice Sheet (FIS) and locally derived material as sources, implying that regional dust emission is not simply a function of sediment supply to the proglacial zone (Pańczyk et al., 2020; Baykal et al., 2021; Waroszewski et al., 2021). Further west along the last EIS margin, glaciofluvial sediments in the exposed North Sea basin are commonly considered as efficient dust sources in LGM dust cycle simulations (Sima et al., 2013; Schaffernicht et al., 2020). Nevertheless, the concept of a northern ice sheet derived source for loess deposits adjacent to the North Sea and Channel basins remains debated and previous work has pointed out the potential for non-glacial contributions from local sources or river floodplains (Fall, 2003; Smalley et al., 2009; Milodowski et al., 2015).

In sum, the role of northern ice sheets in dust generation and loess formation is debated, and the possible connection between abrupt ice sheet meltwater pulses, dust activity and climate remains unclear. However, widespread evidence from multiple archives demonstrates a close connection between dust activity and abrupt climate change (Újvári et al., 2017), and new results reignite the debate about possible northern ice sheet-derived dust sources to Greenland (Újvári et al., 2022). Furthermore, recent high sampling resolution luminescence dating of loess from southeast England shows that dust deposition happened rapidly over MIS 2, with two phases of greatly enhanced accumulation that match the timing of advances and retreats of nearby ice lobes in the North Sea and associated glaciofluvial drainage activity (Stevens et al., 2020). However, proof of the causal links between this episodic LGM loess deposition in NW Europe and ice sheet dynamics is lacking, mainly caused by uncertainty over the sources and transport pathways of this material. Given that this loess in southeast England is preserved exceptionally close to the meltwater drainage route of ice lobes in the western North Sea (Bunce et al., 2022), constraining its sources offers an opportunity to test the role of ice sheet dynamics in proglacial sediment supply and dust activity more widely, as well as the coupling and association of ice sheet-driven dust pulses with climate change. In order to undertake such a test, we first review previously proposed dust sources in the North Sea region for loess in NW Europe. We then present an extensive compilation of published and new sediment source proxy data from these sediments

as well as protosource terranes across Europe. This dataset enables both discrimination between potential dust sources to the loess and also reconstruction of sedimentary pathways into the North Sea region. Against this framework, we present a detailed multi-proxy provenance analysis of high sampling resolution luminescence dated ice marginal loess in southeast England and identify the wider implications for dust activity. Based on this case study, we demonstrate and explore the role of the EIS, and ice sheets generally, on dust production, and the link between ice sheet meltwater events, climate, and high-latitude dust activity in the late Quaternary.

1.1. North Sea ice dynamics, drainage history and loess sources during the Late Pleistocene

During MIS 2, the southern North Sea and Channel basins were largely exposed due to global sea level lowering, and hosted extensive fluvial and glaciofluvial systems that drained sediment rich meltwater from large parts of the British-Irish, Fennoscandian and Alpine Ice Sheets (Fig. 1; Patton et al., 2017). The resulting sediment cover exposed in the North Sea and Channel basins has traditionally been considered as the main dust source for loess in NW Europe (e.g. Perrin et al., 1974; Antoine et al., 2003; Sima et al., 2013; Bunce et al., 2022). Indeed, loess deposits in southern England exhibit a general reduction in both thickness and mean grain size from E-W (Kent – East Devon), implying dust sourcing from the adjacent North Sea basin (Catt and Staines, 1982). Likewise across NW Europe, the source proximal cover sand belt gives way to the south and west to cover loams and then loess, also implying a southerly/south-westerly aeolian transport pathway (e.g., Koster, 2005: Fig. 1). LGM dust cycle simulations also indicate that dust transport pathways over central and western Europe were mainly controlled by east sector winds caused by the high pressure system over the EIS and southwards deflected cyclones (Schaffernicht et al., 2020), both of which would facilitate dust entrainment from the North Sea basin by northeasterly-easterly winds and transport to SE England (Stevens et al., 2020). However, local variability in the geochemical signature of loess deposits along the Channel suggests additional input from local bedrock sources and silt supply from rivers draining southern England (Fall, 2003). Furthermore, Lefort et al. (2019) highlight the importance of katabatic, northerly winds for dust transport in regions proximal to the MIS 2 EIS margin, potentially favoring local source contributions for loess in southern England.

While the concept of a North Sea basin dust source for loess in SE England is generally, but not entirely, agreed upon, what is less clear is how sediment was transported into the North Sea basin and what the proto-sources for this material were (Bunce et al., 2022). Lill and Smalley (1978) proposed glacigenic sediments derived from the last glacial EIS as source for loess deposits in southern England. Indeed, a British Irish Ice Sheet (BIIS) derived dust source is consistent with findings from heavy mineral analyses on last glacial tills and loess deposits in Eastern England (Madgett and Catt, 1978; Bateman and Catt, 2007). Furthermore, Eden (1980) concluded that loess in southeastern England is part of a wider, glacially derived loess belt expanding over Belgium and the Netherlands, based on similarities in the heavy mineral composition. However, the abundance and composition of amphiboles in the loess was taken here to imply a more Scandinavian origin (Eden, 1980). Challenging the concept of northern ice-sheet derived loess more widely, Smalley et al. (2009) proposed a theoretical model that involved sediment transport from Alpine protosources via the last glacial Rhine into the North Sea region. Complicating matters further, a number of studies on loess and loess-like sediments from the Isle of Thanet, SE England suggest local derivation of loess from the underlying Palaeocene Thanet Formation (Pitcher et al., 1954; Catt et al., 1987). Most recently, Milodowski et al. (2015) proposed a temporal change in Thanet loess provenance, initially from reworked Thanet Fm. material but shifting to glacial detritus derived from the North Sea basin, based on variability in mineralogical and grain morphological characteristics of the loess. Thus, at present, a wide range of possible proto-sources and transport pathways for meltwater sediment, dust and loess in southeast England remains plausible, and the cause of enhanced loess deposition during MIS 2, and any link between dustiness and ice sheet dynamics, remains enigmatic. As such, SE England represents an ideal test of the contested role of northern ice sheets in loess and dust generation (Smalley et al., 2009; Baykal et al., 2021), as well as the possible effect of abrupt ice sheet meltwater events on wider dust activity.

New insights from high sampling resolution luminescence dating of loess deposits from Pegwell Bay, SE England allows interpretation of loess accumulation phases in the context of the increasingly well constrained MIS 2 North Sea ice history (Stevens et al., 2020). Loess only began to accumulate over southeast England abruptly from ca. 26–25 ka, after the BIIS and Fennoscandian Ice Sheet (FIS) had coalesced in the North Sea basin (Roberts et al., 2018; Clark et al., 2022) and glacial meltwater transport was redirected southwestwards via the Channel River (Figs. 1 and 2; Patton et al., 2017). Two phases of greatly enhanced dust deposition centered on ca. 25–23.5 ka and 20–19 ka (Fig. 2) match the proposed timing of advances and retreats of the nearby North Sea Lobe (NSL; Sejrup et al., 2016; Roberts et al., 2018; Evans et al., 2021; Clark et al., 2022), which Stevens et al. (2020) suggest were likely associated with major meltwater floods and increased sediment supply in the proglacial North Sea basin. These findings provide a framework for interpreting potential dust sources for loess in southeast England, and potentially more widely in NW Europe, as well as the role of northern ice sheets in wider dust generation and dust-climate coupling. Furthermore, new provenance data from shallow marine sands of the Palaeocene Thanet Formation (Stevens and Baykal, 2021) allow for testing the impact of local sources for this loess. As such, here we conduct an extensive analysis of published and new sediment source proxy data from potential dust sources in the North Sea region as well as zircon U–Pb dating results from basement in NW Europe. We use this database to differentiate between dust source sediments, identify protosource terranes and reconstruct sedimentary pathways into the North Sea region. Based on this framework, we undertake a multi-method provenance study of MIS 2 loess at Pegwell Bay, SE England, combining detrital zircon U–Pb dating with bulk Nd isotope and heavy mineral assemblage data to source fingerprint the loess and assign it to potential source sediments from the North Sea basin. Moreover, we use SEM imagery to analyze the shape and surface of detrital quartz grains and gain further insight into the processes involved during sediment production and transport.

2. Sampling sites and methods

2.1. Loess at Pegwell Bay, SE England

Loess deposits are exposed along the North Sea cliffs of Pegwell Bay, East Kent (Figs. 1 and 3), unconformably overlying sands of the Palaeocene Thanet Formation or brecciated Cretaceous Chalk (Pitcher et al., 1954). Stevens et al. (2020) reported new sedimentological and chronological data from a 3.6 m thick profile (51.328N, 1.370E) comprising the region's typical, distinct lithological succession (Fig. 3). The loess sequence is capped by a grey-brown modern/Holocene soil unit (0–0.66 m) overlying brownish, non-calcareous loess (0.66–1.78 m). The lower boundary of this upper

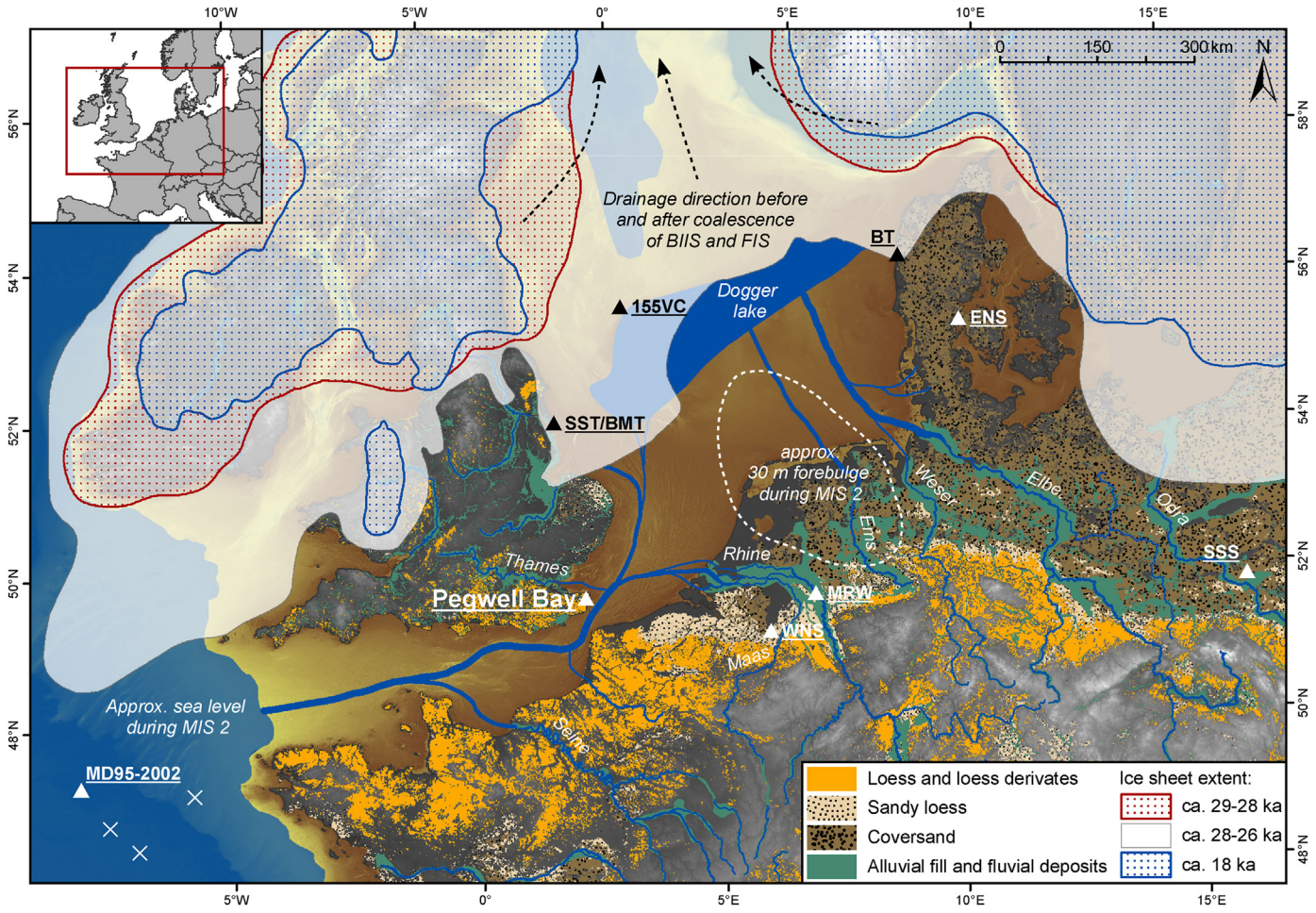

Fig. 1. Map of NW Europe showing the distribution of loess and coversand (Bertran et al., 2021) and alluvial fill and fluvial deposits (Lehmkuhl et al., 2021). Generalized ice sheet extents (based on Hughes et al. (2016); Smedley et al. (2017); Roberts et al. (2018); Scourse et al. (2019)), MIS 2 glacioisostatic forebulge (Busschers et al., 2007), proposed drainage in the exposed North Sea, Pegwell Bay and other sampling sites noted. Labels for WNS and ENS indicate approximate locations of grouped samples. White crosses indicate marine coring sites MD03-2690, MD03-2688 and MD03-2695 (from west to east). North Sea bathymetry downloaded from EMODnet.

loess unit is marked by a sharp transition to the underlying buff coloured, calcareous lower loess unit (1.78–3.40 m), which in turn rests on shallow marine to estuarine sands of the Thanet Formation (deeper than c. 3.40 m). Luminescence dating and Bayesian age modelling results from Stevens et al. (2020) are shown in Figs. 2 and 3.

For the present study, 10 loess samples (taken every 20–30 cm) have been selected from the previously luminescence dated loess section at Pegwell Bay for Nd isotope analysis (Fig. 2, Appendix A: Table 1). Moreover, 2 loess samples have been selected for detrital zircon U–Pb dating, heavy mineral and SEM analyses: PB210-230 (2.10–2.30 m below surface) corresponding to the end of the first phase of enhanced accumulation or beginning of reduced dust deposition (range reflects chronological uncertainties) and PB130-150 (1.30–1.50 m below surface) corresponding to the second phase of enhanced dust accumulation (Figs. 2 and 3).

2.2. Reference samples from potential source sediments and primary protosource regions

In order to evaluate previously proposed source scenarios for the loess at Pegwell Bay and to constrain pathways for sediment transport into the North Sea region we collected 5 reference samples from potential dust source sediments. Late Palaeocene shallow marine to estuarine sands from the Thanet Formation underlying the loess at Pegwell Bay have been sampled ca. 1 m below the contact to the lower loess unit (PBTF: 51.328N, 1.370E; Figs. 1 and 3; Stevens and Baykal, 2021). BIIS derived Basement Till (BMT) and Skipsea Till (SST) units were sampled along the North Sea coastline near Holderness in Yorkshire, eastern England (Fig. 1; 53.668N, 0.110E and 53.996N, 0.209W respectively). The chronological framework based on luminescence dating of glacigenic and glacial lake deposits exposed along the Holderness coastline suggests the Basement Till dates to pre 26–24 ka and the Skipsea Till 26–22 ka, both deposited during late last glacial North Sea Lobe advances (Bateman et al., 2015, 2018; Evans et al., 2021). Sample 155VC is taken from a sediment core initially sampled by the BRITICE-CHRONO project during cruise JC 123 in 2015. The core was collected from glaciolacustrine sediments of Dogger lake in a basin between moraines on the northern edge of the Dogger Bank in the central North Sea (55.38N, 1.32E). The sample reported here was taken from a core depth of 499–518 cm, while a sample from a depth of 357 cm was previously luminescence dated to 23.1 ± 2.3 ka (Roberts et al., 2018). Modern Rhine sediment was sampled from an exposed riverbank near Werrich, Germany (Fig. 1; MRW: 51.660N,

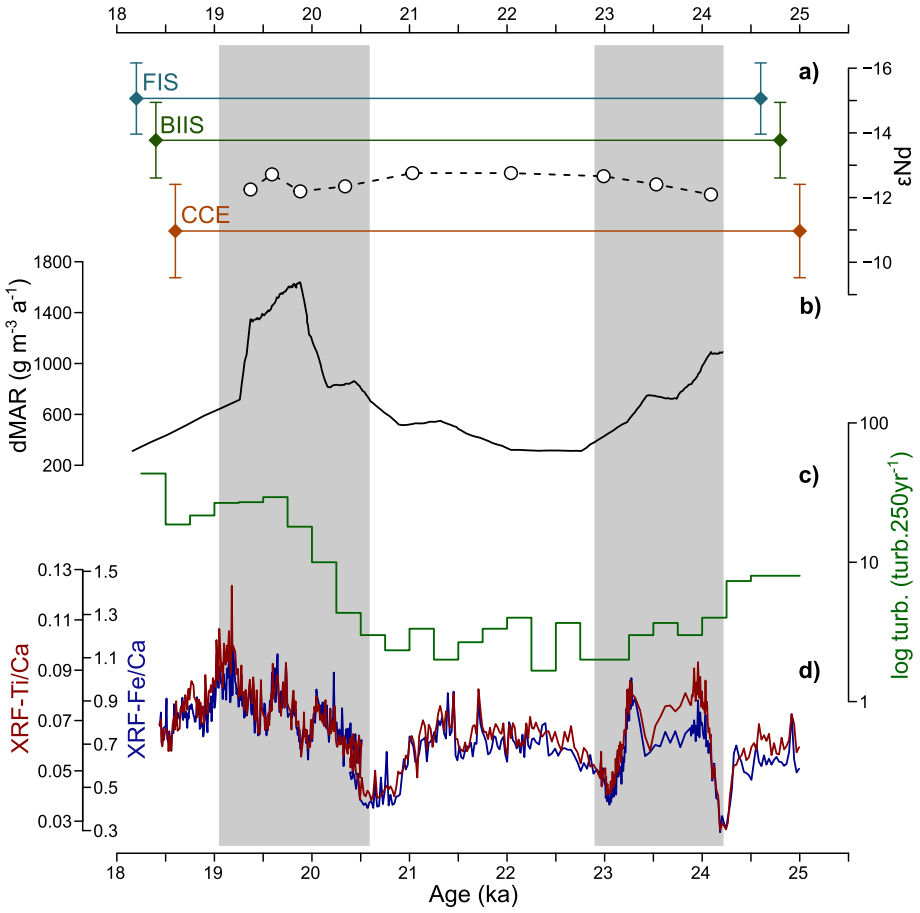

Fig. 2. a) Nd isotope record of loess at Pegwell Bay over time compared to grouped reference data from glacigenic samples around the FIS and BIIS margin and fluvial sediment samples from rivers draining central Continental Europe (CCE), see Appendix A: Table 1 for values and references; b) Pegwell Bay dust (d) MAR (see Fig. 1 for location; Stevens et al., 2020); c) Turbidite flux off the Channel River from marine cores MD03-2690, MD03-2688 and MD03-2695 (marked by white crosses in Fig. 1; Toucanne et al., 2012); d) XRF Ti/Ca (red) and XRF-Fe/Ca (blue) ratios for core MD95-2002 (see Fig. 1 for location) as proxies for terrigenous-siliclastic input, and by extension Channel River runoff (see Fig. 1 for location; Toucanne et al., 2015) while minimum values around 24 ka indicate the impact of authigenic calcite precipitation during Heinrich event 2 (Hemming, 2004). Grey shaded areas indicate phases of peak dust accumulation at Pegwell Bay. (For interpretation of the references to colour in this figure legend, the reader is referred to the Web version of this article.)

6.508E). Moreover, we complement the new loess source analysis with published data from other Cenozoic sediments across the North Sea region (Figs. 1 and 4), including Late Pleistocene sandur sediments from the Northern European Plain (SSS; Baykal et al., 2021), the Late Pleistocene Black Till from Denmark (BT; Knudsen et al., 2009) and grouped data from Quaternary Rhine terrace sediments (RTe; 550–250 ka; Krippner and Bahlburg, 2013), Neogene marine paralic sediments in the western North Sea basin (WNS; Verhaegen et al., 2021) and Miocene fluvio-deltaic sediments from the eastern North Sea basin (ENS; Olivarius et al., 2014).

In order to retrace protosources of potential dust source sediments in the North Sea region and loess in southeast England we also compiled extensive published zircon U–Pb data from basement terranes across Europe (compilation expanded after Bingen and Solli, 2009; Fairey et al., 2018; Baykal et al., 2021; Bingen et al., 2021; Stevens and Baykal, 2021, Figs. 5 and 6). Assembled data includes both detrital zircon U–Pb data from sedimentary rocks as well as zircon U–Pb ages from igneous rocks, with only the reported age included for the latter to avoid overrepresentation of certain rocks in the terrane spectra. See Appendix A for the full reference list of the compilation.

2.3. Detrital zircon U–Pb dating

Detrital zircon grains were separated from 1 to 2 kg of bulk material from the loess samples (PB130-150; PB210-230) and new reference samples (SST; 155VC) using a Wilfley table, heavy liquids (methylene iodide), and a Frantz magnetic separator. A large proportion of the non-magnetic heavy mineral fraction was mounted in epoxy together with fragments or loose grains of Sri Lanka (Gehrels et al., 2008), FC-1 (Black et al., 2003), and R33 (Black et al., 2004) zircon used as primary standards. The mounts were sanded down to a depth of ~20 μm, polished, and backscattered electron (BSE) images were generated using a Hitachi 3400N scanning electron microscope (SEM). Zircon U–Pb dating was conducted by laser ablation inductively coupled plasma mass spectrometry (LA-ICPMS) at the Arizona LaserChron Center (Gehrels et al., 2006, 2008; Gehrels and Pecha, 2014; Pullen et al., 2018) using a Photon Machines Analyte G2 excimer laser equipped with a HelEx ablation cell coupled to a Thermo Element2 HR ICPMS. The laser beam diameter was 12 μm with an energy density of ~7 J/cm^2, a 7 Hz repetition rate and an ablation time of 10 s resulting in ablation pits of 12 μm in depth. The data was reduced utilizing an in-house

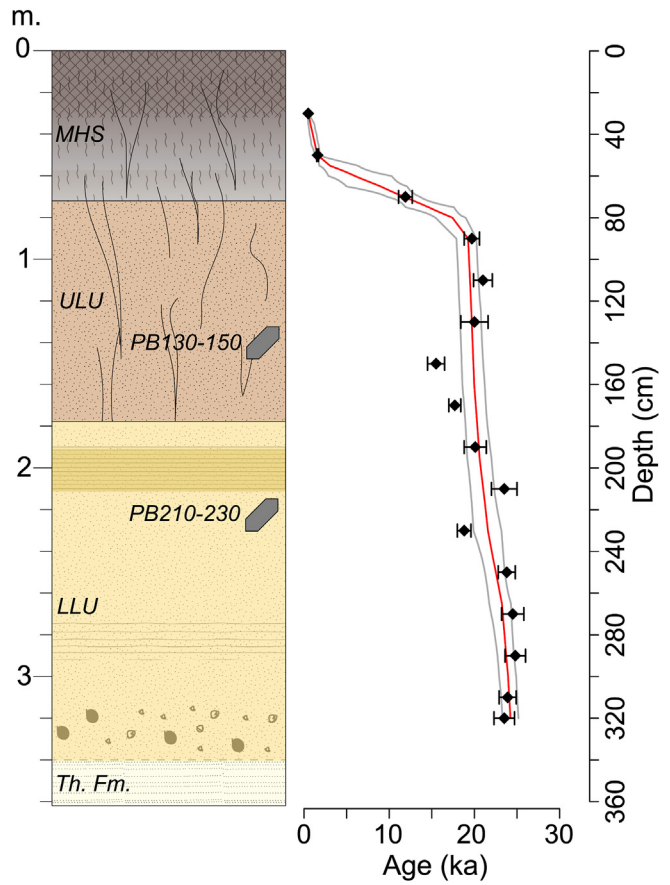

Fig. 3. Stratigraphic log of the Pegwell Bay loess section, subdivided into three units: modern/Holocene soil (MHS), upper loess unit (ULU) and lower loess unit (LLU), overlying the Thanet Fm (Th. Fm.; modified after Stevens et al. (2020)) in relation to age depth model based on quartz OSL ages (Stevens et al., 2020). Sampling positions for detrital zircon U–Pb dating, heavy mineral and SEM analyses are indicated for the loess only.

python decoding routine and Excel spreadsheet (E2agecalc; see Baykal et al., 2021 for details). The "Best Age" used for plotting and interpretation was defined as $^{206}Pb/^{236}U$ age for analyses with $^{206}Pb/^{236}U$ age <900 Ma and $^{206}Pb/^{207}Pb$ age for analyses with $^{206}Pb/^{236}U$ ages >900 Ma. Concordance was based on $^{206}Pb/^{236}U$ age/$^{206}Pb/^{207}Pb$ age. This value was not reported for $^{206}Pb/^{236}U$ ages <400 Ma because of large uncertainty in the $^{206}Pb/^{207}Pb$ age. Analyses where $^{206}Pb/^{236}U$ ages exceed 400 Ma and with >20% discordance or >5% reverse discordance were not included in further analyses. Uncertainties for individual measurements are reported at the 1-sigma level including only measurement errors.

Generally, the reproducibility of detrital zircon U–Pb age distributions and their accuracy in modelling sediment provenance increases with the number of analyzed grains (n) (Pullen et al., 2014). Detrital zircon age distributions with $n \geq 117$ should reflect the presence or absence of age components accounting for >5% of the total population at a 95% certainty (Vermeesch, 2004). Yet, substantially more analyzed grains are needed to compare the relative proportions of individual age components. For the present detrital zircon age study we generated large n data sets (aiming for >300 analyzed grains) that facilitate such semi-quantitative comparison of relative abundance of zircon age components (Pullen et al., 2014; Nie et al., 2018; Zhang et al., 2021).

Zircon age distributions of different samples and published data assembled from potential source sediments as well as proto-source terranes were visualized and compared using Kernel Density Estimation (KDE) diagrams (Vermeesch, 2012). To facilitate multi-sample comparisons of detrital zircon U–Pb age distributions, we applied multi-dimensional scaling (MDS), a statistical tool that plots high-dimensional datasets into a lower dimensional subspace. The resulting two dimensional "map" displays clusters of similar samples based on Kolmogorov-Smirnov statistics (Stevens et al., 2013; Vermeesch, 2013).

2.4. Heavy mineral analyses

Heavy mineral fractions were separated from the loess (PB140; PB220) and reference samples (PBTF; BMT; SST; 155VC; MRW) using LST heavy liquid (density: 2.67 g/cm^3). Automated mineralogical analysis was performed at the Mineral and Materials Characterization Facility in the Department of Geology and Geological Engineering at the Colorado School of Mines using a Tescan-VEGA-3 Model LMU VP-SEM platform combined with the TIMA3 (Tescan Integrated Mineral Analyzer) control program. Four energy dispersive X-ray (EDX) spectrometers acquired element spectra with a stepping distance of 5 μm at an acceleration voltage of 25 kV and a beam intensity of 14. Mineral phases were identified at each acquisition point by comparison of measured EDX spectra with known spectra and compositional mineral maps were then generated. Results were output by the TIMA3 software as a spreadsheet giving the volume percentage and number of grains of each identified mineral. Following this approach, large numbers of mineral grains can be identified rapidly to increase statistical representativity, although detailed compositional analysis is not feasible. For the present study, the number of heavy mineral grains counted per sample varies from 3300 to 55,100.

2.5. Nd isotope analyses

The Nd isotopic composition of the 10 Pegwell Bay loess samples as well as SST, BMT and 155VC were analyzed at ALS Scandinavia in Luleå, Sweden. Dried, fine-grained fractions (<125 μm) were milled using a laboratory mill (LUN-MEK, Mariehamn, Åland) and the entire material was prepared for analysis by lithium metaborate fusion (Rodushkin et al., 2000). The Nd fraction was purified by two column ion exchange chromatography first using DOWEX 50W X-8-200 (Sigma-Aldrich, Stockholm, Sweden) resin to separate REEs from sample matrix and then Ln-850-A (Trisken International, Bruz, France) resin for Nd/Sm separation (Makishima et al., 2008). Analyte recoveries and purification efficiency was assured by ICP-SFMS analysis of digests and purified fractions. Nd isotopic measurements were carried out by MC-ICP-MS (NEPTUNE Plus, ThermoScientific) using internal standardization and external calibration with bracketing analyses of SRMs JB-2 and MERCK-ND solution.

Samples PBTF and MRW were analyzed at the Key Laboratory of Mineral Resources in Western China (Gansu Province), Lanzhou University, China. Firstly, the samples were pulverized to >200 μm and then, carbonate and organic matter were removed using 0.5 mol L-1 acetic acid (CH_3COOH) and 10% hydrogen peroxide (H_2O_2), respectively. Sample material was dissolved using $HF–HNO_3$ and then separated by conventional ion-exchange techniques (Bao et al., 2018). Nd measurements were carried out through MC-ICP-MS (Nu Instruments, UK). Isotopic ratios of $^{146}Nd/^{144}Nd = 0.7219$ were used to correct mass bias. During the analysis, the JNDi-1 was selected as the solution standard of the Nd isotope, and repeated analyses gave $^{143}Nd/^{144}Nd$ ratios of 0.512112 ± 0.000007 (n = 29), in full agreement with the

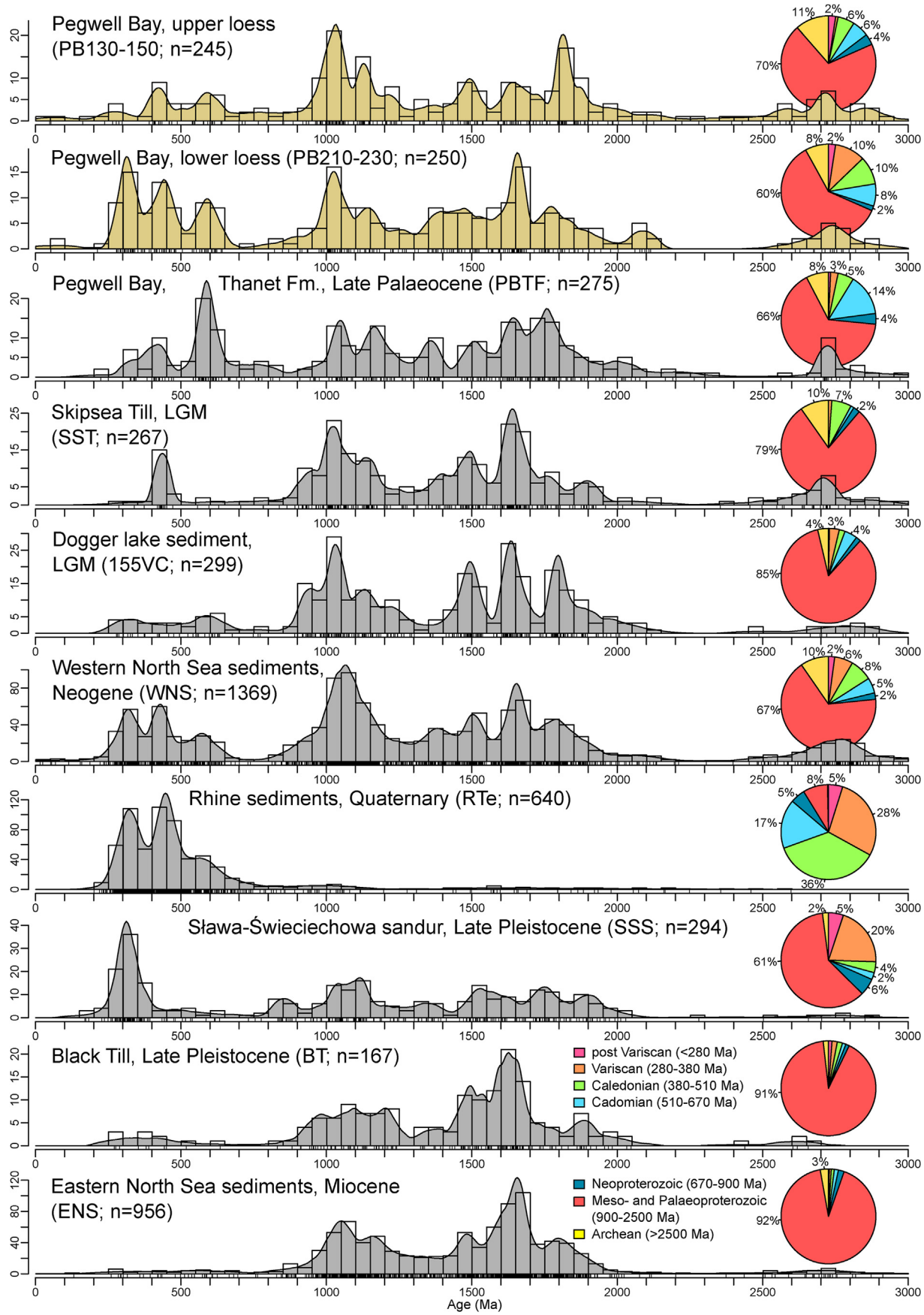
Pegwell Bay, upper loess
(PB130-150; n=245)
11%
2%
6%
6%
4%
70%
Pegwell Bay, lower loess (PB210-230; n=250)
8%
2%
10%
10%
8%
2%
60%
Pegwell Bay, Thanet Fm., Late Palaeocene (PBTF; n=275)
8%
3%
5%
14%
4%
66%
Skipsea Till, LGM
(SST; n=267)
10%
7%
2%
79%
Dogger lake sediment,
LGM (155VC; n=299)
4%
3%
4%
85%
Western North Sea sediments,
Neogene (WNS; n=1369)
10%
2%
6%
8%
5%
2%
67%
Rhine sediments, Quaternary (RTe; n=640)
8%
5%
5%
28%
17%
36%
Sława-Świeciechowa sandur, Late Pleistocene (SSS; n=294)
2%
5%
20%
61%
4%
2%
6%
Black Till, Late Pleistocene (BT; n=167)
post Variscan (<280 Ma)
Variscan (280-380 Ma)
Caledonian (380-510 Ma)
Cadomian (510-670 Ma)
91%
Eastern North Sea sediments, Miocene
(ENS; n=956)
3%
Neoproterozoic (670-900 Ma)
Meso- and Palaeoproterozoic
(900-2500 Ma)
Archean (>2500 Ma)
92%
0
500
1000
1500
2000
2500
3000
Age (Ma)

recommended value of 0.512115 (Tanaka et al., 2000). Two international standards (BCR-2 and AGV-2) were included in the analysis. Standard BCR-2 and AGV-2 gave $^{143}Nd/^{144}Nd$ values of 0.512642 ± 0.000005 (n = 3) and 0.512790 ± 0.000004 (n = 2), agreeing with the certified values of 0.512635 ± 0.000029 and 0.512786 ± 0.000014 (Jochum et al., 2016), respectively.

All measured and previously published data presented here are reported in εNd notation using $(^{143}Nd/^{144}Nd)_{CHUR} = 0.512638$ (Jacobsen and Wasserburg, 1980).

2.6. SEM analyses of detrital quartz grain shape and surface

The light mineral fractions of loess (PB120; PB240) and reference samples (PBTF) were separated using LST heavy liquid (density: 2.65 g/cm^3). Selected grains were mounted onto double-sided adhesives, coated with a 15 nm gold layer, and imaged using a JEOL JSM-6510 LV scanning electron microscope (SEM) with a magnification range of X130 − X1800 at the Upstream Laboratory of INA oil company, Zagreb. More than 400 different grains were photographed and images that show entire quartz grains were selected to analyze their shape and detailed surface texture. Quartz grain surface microtexture classification and terminology used in the present study are based on Mahaney (1995, 2002) and Strand et al. (2003).

3. Results

3.1. Zircon U–Pb dating

Zircon grains recovered from the Pegwell Bay loess samples PB130-150 and PB210-230 yielded 245 and 250 concordant ages, respectively (Fig. 4). Late Neoproterozoic and Phanerozoic zircon ages reported from these samples show significant differences in distribution and abundance (Fig. 4). Sample PB210-230 from the lower loess exhibits a dominant Carboniferous-early Permian age population at ca. 310 Ma along with substantial amounts of Ordovician-early Devonian zircon ages at ca. 450 Ma and late Neoproterozoic zircon ages at ca. 600 Ma, all adding up to 28% of the total distribution. In contrast, sample PB130-150 from the upper loess contains very few late Carboniferous-early Permian age zircon grains and both Ordovician-early Devonian zircon ages at ca. 420 Ma and Late Neoproterozoic zircon ages at ca. 600 Ma are somewhat less abundant, all adding up to 16% of the total distribution. Both PB210-230 and PB130-150 show similar distributions of Meso- and Palaeoproterozoic zircon ages that form significant age peaks at ca. 1.05 Ga, 1.15 Ga, 1.5 Ga, 1.65 Ga and 1.8 Ga, adding up to 60% and 70% of the total distributions, respectively. The 1.65 Ga zircon age component is more abundant in sample PB210-230 while zircon ages of 1.8 Ga form a more important peak in sample PB130-150. Archean age zircon grains recovered from samples PB210-230 and PB130-150 cluster at ca. 2.75 Ga, accounting for 8% and 11% of the total age distributions, respectively.

Zircon U–Pb dating of the LGM Skipsea Till sample (SST) yielded 267 zircon ages that passed the discordancy criteria (Fig. 4). Phanerozoic and late Neoproterozoic ages are mostly limited to Silurian age, forming a single, well constrained age peak at ca. 440 Ma that accounts for 6% of the total distribution. Meso- and Palaeoproterozoic zircon ages are dominated by the two most abundant age peaks centered on ca. 1.03 Ga and 1.65 Ga, while somewhat smaller age peaks are present at ca. 1.15 Ga and 1.5 Ga, all adding up to 79% of the total age distribution. Archean zircon ages cluster at ca. 2.7 Ga and total 10% of the ages.

Zircon grains recovered from the LGM Dogger lake sediment sample (155VC) yielded 299 concordant ages (Fig. 4). Phanerozoic and late Neoproterozoic zircon ages are widely scattered between 280 and 780 Ma, adding up to 11% of the total age distribution. Meso- and Palaeoproterozoic zircon ages total 85% of the age spectrum, characterized by 4 most abundant age peaks centered on ca. 1.03 Ga, 1.5 Ga, 1.65 Ga and 1.8 Ga. Sporadic Archean zircon ages are present between 2.65 and 2.9 Ga, adding up to 4% of the total distribution.

The results from the new samples presented here are shown alongside previously published detrital zircon U–Pb age data from other possible source areas in Fig. 4 (see references for description): Late Palaeocene Thanet Fm. shallow marine to estuarine sands from Pegwell Bay (PBTF; Stevens and Baykal, 2021), Neogene marine/paralic sediments from the southwestern North Sea (WNS; Verhaegen et al., 2021), Quaternary Rhine sediments (RTe; Krippner and Bahlburg, 2013), Late Pleistocene sandur sediments from the Northern European Plain (SSS; Baykal et al., 2021), the Late Pleistocene Black Till from Denmark (BT; Knudsen et al., 2009) and Miocene deltaic sediments from the southeastern North Sea basin (ENS; Olivarius et al., 2014).

3.2. Heavy mineral assemblages

The analyzed loess and reference samples consist of similar qualitative heavy mineral compositions (Fig. 5), here subdivided based on Morton and Hallsworth (2007) into most stable (zircon, tourmaline, rutile, monazite, apatite and garnet), less stable (staurolite, kyanite/sillimanite/andalusite, sphene, epidote and hornblende) and least stable minerals (clinopyroxenes, orthopyroxenes and olivine in sample MRW). The relative proportions of the different minerals exhibit considerable variation amongst the analyzed samples, mostly corresponding to the enrichment of the ultrastable minerals as expressed by varying ZTR maturity index values. This value is relatively consistent for the two loess samples (PB140: 39.8; PB220: 36.6) while large differences exist between high ZTR values of the Palaeocene Thanet Fm (PBTF: 78) and the Skipsea Till samples (SST: 57.3) and lower ZTR values detected for the other reference samples (BMT: 26; 155VC: 20; MRW: 18.4). In the two loess samples, the “most stable” minerals are dominated by rutile (27%) followed by similar proportions of zircon (5–7%) and tourmaline (5–6%), while apatite is more abundant in PB220 (10%) than in PB140 (5%). Similarly, the potential source sediment samples are all dominated by rutile, followed by varying proportions of zircon, tourmaline and apatite while MRW stands out with relatively low zircon abundance but elevated tourmaline and apatite contents (Fig. 5). “Less stable” mineral (sphene, epidote and hornblende) contents are rather consistent between the loess samples, BMT, 155VC and MRW, accounting for 37–54% of the total spectrum, while depleted in samples PBTF (5%) and SST (14%). The proportion of the “least stable” clino- and orthopyroxenes is consistently low in the two loess samples (8–9%) and varies strongly between the reference samples (PBTF: 3%; SST: 16%; BMT: 25%; 155VC: 18%; MRW: 20%). Olivine was only detected in sample MRW (3%).

Fig. 4. Kernel density estimate (KDE) plots (bandwidth = 25; Vermeesch, 2012) and pie charts of detrital zircon U–Pb ages from loess at Pegwell Bay (PB130-150; PB210-230; this study), Palaeocene Thanet Fm. sands (PBTF; Stevens and Baykal, 2021), the LGM Skipsea Till (SST; this study); LGM Dogger lake sediment (155VC; this study), Neogene sediments in the southwestern North Sea basin (WNS; Verhaegen et al., 2021), Quaternary Rhine sediments (RTe; Krippner and Bahlburg, 2013), Late Pleistocene sandur sediments from the Northern European Plain (SSS; Baykal et al., 2021), the Late Pleistocene Black Till (BT; Knudsen et al., 2009) and Miocene deltaic sediments in the southeastern North Sea basin (ENS; Olivarius et al., 2014).

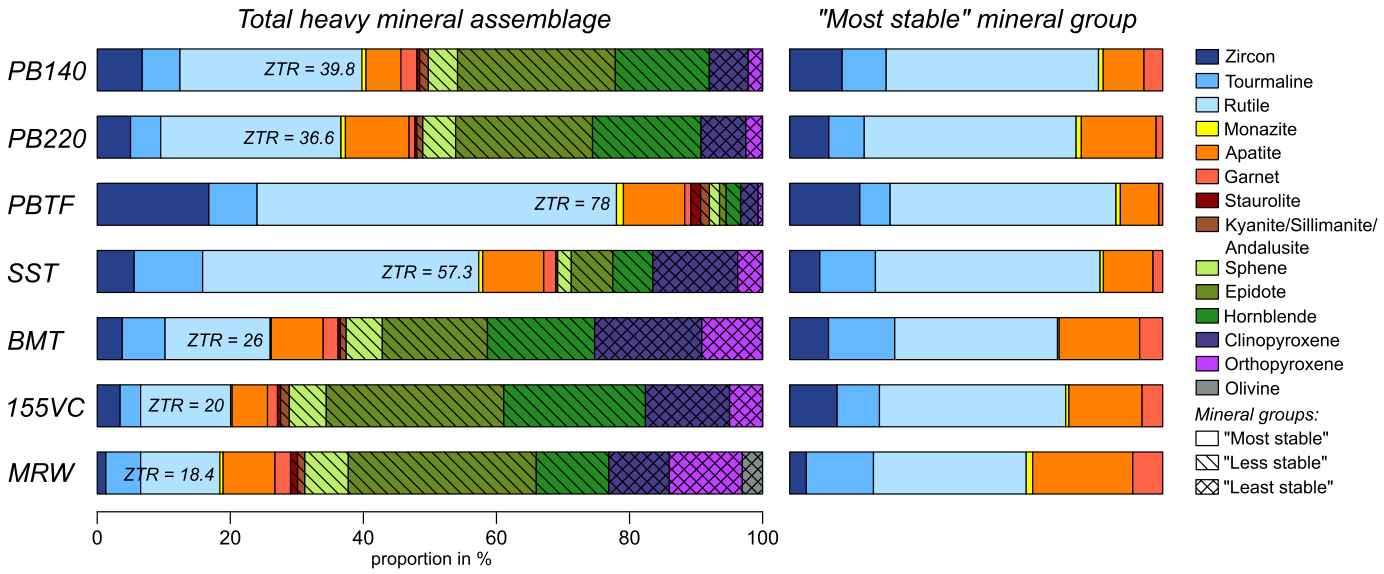

Fig. 5. Stacked bar chart of the heavy mineral composition of two Pegwell Bay loess samples (PB140; PB220), Thanet Fm. sands (PBTF), Skipsea Till (SST), Basement Till (BMT), Dogger lake sediment (155VC) and modern Rhine sediments (MRW). Total heavy mineral spectrum shown on the left grouped according to stability based on Morton and Hallsworth (2007), normalized "most stable" mineral group shown on the right.

3.3. Nd isotopes

Nd isotope measurements from the loess at Pegwell Bay and potential source sediments are shown in Fig. 2 and listed in Appendix A: Table 1. The 10 loess samples show consistent εNd values over the recorded time slice ranging from −12.1 to −13.1. Sample PBTF from Thanet Fm. shallow marine to estuarine sands yielded εNd = −12.3. Sample 155VC from Dogger lake sediments yielded εNd = −14.4. εNd values from the Skipsea and Basement till samples (SST: −14.3; BMT: −15.1) were grouped with published data from till samples from Yorkshire and Norfolk (Toucanne et al., 2015), averaging εNd = −13.8 for BIIS derived detritus. The εNd value from modern Rhine sediments (MRW: −8.9) was grouped with published data from fluvial sediments carried by rivers draining central Continental Europe (Toucanne et al., 2015; Freslon et al., 2014), averaging εNd = −11.0. Moreover, this data was compared with published data from glacigenic sediment samples collected along the FIS margin (average εNd = −15.1; Toucanne et al., 2015).

3.4. SEM analysis of quartz grain morphology and surfaces

Results from SEM image analysis of quartz grains from the samples PB120, PB240 and PBTF are presented in Fig. 6. The two loess samples PB120 and PB240 predominantly consist of angular to subangular grains (Fig. 6 A & E) and about 20% of the grains are marked by subparallel linear, radial or conchoidal fractures (Fig. 6 B, C, D, F, G, H). The proportion of angular grains is somewhat larger in sample PB120 compared to PB240 and the aforementioned surface features are more pronounced. Moreover, the sporadic occurrence of cavernous craters and V-shaped percussion marks is observed amongst grains from sample PB120 (Fig. 6 B & D). Sample PBTF predominantly consists of rounded to sub-angular grains with smoothed edges and medium to high relief, and distinctly weathered surfaces (Fig. 6 I–K). V-shaped percussion marks are also observed, albeit rarely (Fig. 6 L).

4. Discussion

Prior to discussion of specific Late Pleistocene dust source sediments and transport pathways for loess in southeast England and the wider implications for understanding the role of ice sheets in dust generation and abrupt dust and climate change coupling, we first consider the likely primary crustal origins (protosources) for this loess and its potential source sediments in the North Sea basin. In addition to enabling understanding loess and dust sources, this compilation and review aims at facilitating provenance analyses for Cenozoic sediments more widely in NW Europe and especially the North Sea basin.

4.1. Protosources of loess and Cenozoic-Quaternary NW European sediments from zircon U–Pb ages

The oldest crust in the potential source regions is represented by Archean basement in Northern Britain (Laurentia) and Fennoscandia (Baltica), with particularly significant proportions of late Archean zircon ages (c. 2.75 Ga) compiled from Laurentian basement (Fig. 7: 1). Across Baltica, late Archean basement rocks are mostly restricted to northern and eastern terranes (Fig. 7: 14; Bogdanova et al., 2008). During the Palaeo- and Mesoproterozoic, basement terranes in Laurentia and Baltica were subjected to multiple contemporaneous phases of enhanced magmatic activity at ca. 1.8, 1.65 and 1.5 Ga (Fig. 7: 1, 5–10, 12, 13), while terranes in Continental Europe and central to southern Britain remained less affected during this period. The subsequent assembly of supercontinent Rodinia (1.3–0.9 Ga; Li et al., 2008) involved collision of Amazonia with Laurentia and Baltica, forming the Grenvillian (c. 1.15–1.05 Ga) and Sveconorwegian orogens (c. 1.06–0.9 Ga), respectively (Bingen et al., 2021). During this continental amalgamation, detritus derived from the orogenic belts accumulated near the junction between these large continental blocks, as preserved in allochthonous sedimentary rocks in the northern Scandinavian Caledonides (Kirkland et al., 2007; Bingen and Solli, 2009).

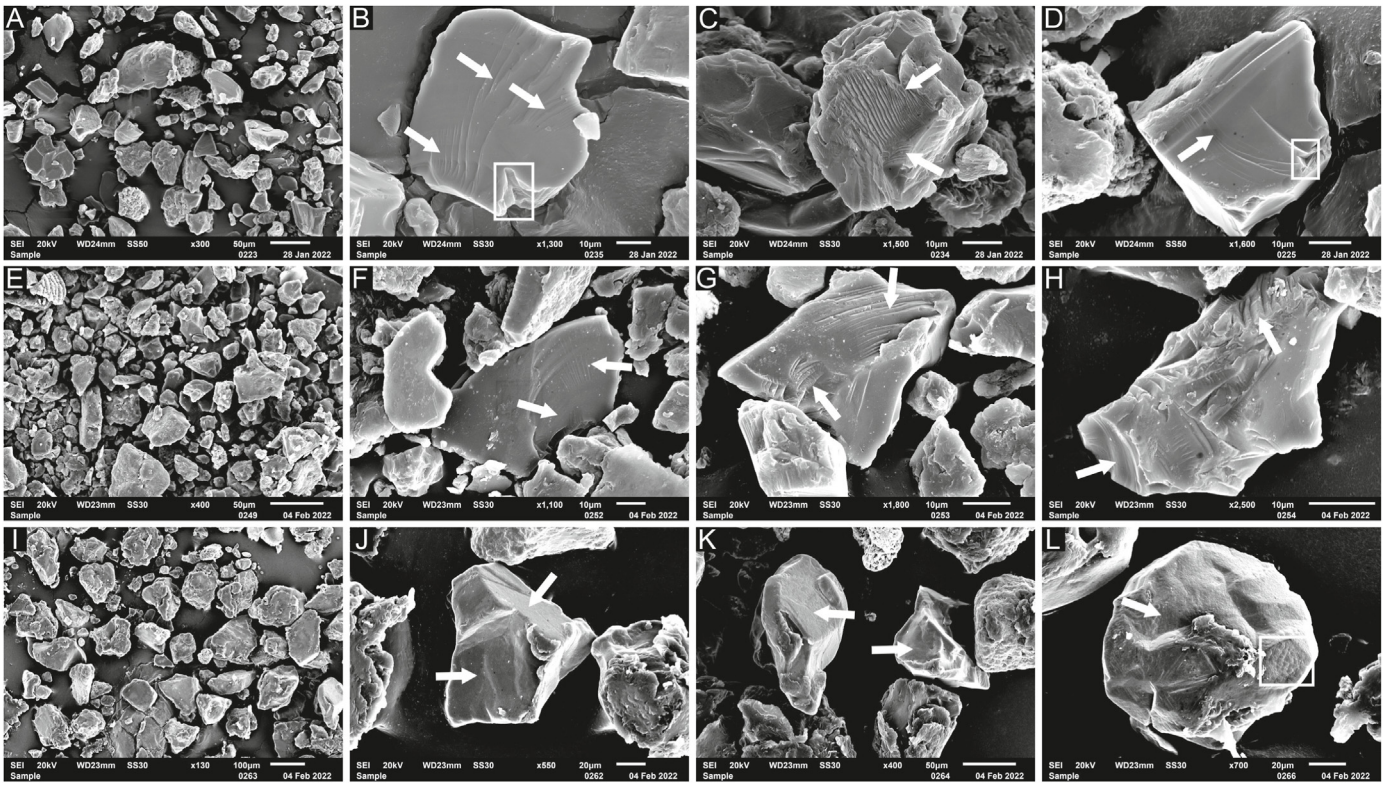

Fig. 6. A: Sample PB120: overview of the sample under lower magnification. Angular and sub-angular grains predominate in the sample over sub-rounded grains. B: Sample PB120: grain with low relief and rounded corners with subparallel linear fractures marked with arrows. Cavernous crater is visible in rectangle. C: Sample PB120: sub-angular grain with sharp edges, fracture faces and high frequency fractures (a mix of conchoidal and subparallel linear fractures) marked with arrows. D: Sample PB120: angular grain with subparallel linear fractures marked with arrow and major V-shaped percussion mark in rectangle. E: Sample PB240: overview of the sample under lower magnification. Angular and sub-angular grains predominate in the sample. F: Sample PB240: grain with conchoidal fracture surface marked with an arrow pointing to the right and radial fractures on top of it marked with an arrow pointing to the left. G: Sample PB240: angular grain with sharp edges, fracture faces and combination of conchoidal fractures and subparallel linear fractures marked with arrows. H: Sample PB240: conchoidal fracture marked with an arrow pointing to the right and linear steps marked with an arrow pointing to the top. The grain surface is almost completely covered with grooves of different lengths and depths. I: Sample PBTF: overview of the sample under lower magnification. There is an almost equal ratio of sub-angular and sub-rounded grains in the sample. J: Sample PBTF: Grain with slightly smoothened edges and fracture surfaces marked with arrows. K: Sample PBTF: Grains with fracture surfaces marked with arrows. Grain on the left has rounded edges. L: Sample PBTF: Well-rounded grain with abraded surface, fracture face marked with an arrow and most likely a set of V-shaped percussion marks in rectangle.

This similar history and the potential for ancient sediment mixing between Laurentia and terranes in Baltica is reflected by common Palaeo- and Mesoproterozoic zircon U–Pb age peaks of the Cenozoic North Sea basin sediments likely derived, at least in part, from these terranes (Fig. 4: PBTF, SST, 155VC, BT, ENS). By contrast, late Archean age zircons are present in sediments derived from British basement (PBTF, SST, 155VC), while absent in the Fennoscandian derived sediments (BT, ENS, SSS) presented here. In particular, the lack of these grains in FIS derived glaciofluvial sediments in the North Sea region (BT) and Northern European Plain (SSS) implies that ice streams eroding late Archean basement units in eastern Baltica are mostly drained towards the Eastern European Plain (Soulet et al., 2013; Patton et al., 2017), as confirmed by the presence of late Archean age grains in fluvial sediments draining the eastern sector of the former Eurasian Ice Sheet, as well as other Quaternary sediments across the region (Wang et al., 2011; Pańczyk et al., 2020; Költringer et al., 2022). Moreover, the BIIS derived Skipsea Till (SST) and glacial lake sediments from the western North Sea (155VC) exhibit a relatively more important Grenvillian/Sveconorwegian age peak at ca. 1.05 Ga, as compared to the Black Till and Miocene fluviodeltaic sands in the eastern North Sea (ENS; Olivarius et al., 2014), which are derived exclusively from Scandinavian terranes.

After a tectonically rather quiescent period recorded as a "Neoproterozoic gap" in zircon ages (Figs. 4 and 7), multiple younger phases of magmatic activity affected basement rocks in the protosource regions. During the late Neoproterozoic, the Cadomian orogeny (670-510 Ma) occurred along the northern margin of Gondwana, and is preserved in rocks across terranes in central to southern Britain and Continental Europe (Linnemann et al., 2008, Fig. 7: 2–4, 15–26), while absent in Laurentia and Baltica. The subsequent early Phanerozoic collision of Laurentia, Baltica and Avalonia caused by closure of the Iapetus ocean (summarized as Caledonian orogeny; 510-380 Ma) (McKerrow et al., 2000) is well represented in the Scottish and Scandinavian Caledonides. Indeed, the detrital zircon age distribution obtained from the BIIS derived Skipsea Till (Fig. 4: SST) exhibits a significant Caledonian age peak, entirely consistent with sourcing from Northern Britain (Laurentia). However, zircon grains equivalent in age to the Caledonian orogeny are substantially more abundant across Peri-Gondwanan terranes (Fig. 7: 18, 19, 20, 26), suggesting Continental Europe is also a likely source for grains of this age. Furthermore, the Fennoscandian derived Black Till shows a conspicuous absence of zircons of this age (Fig. 4). The youngest zircon age component detected in the loess and potential source sediments overlaps in age with the Variscan orogeny (ca. 380-280 Ma). This event is recorded by widespread zircon growth along the Variscan belt in Continental Europe (Fig. 7) and the SW British Isles (Neace et al., 2016; Stephan et al., 2019), while other terranes remained rather unaffected. This southern provenance is consistent with the abundance of Variscan

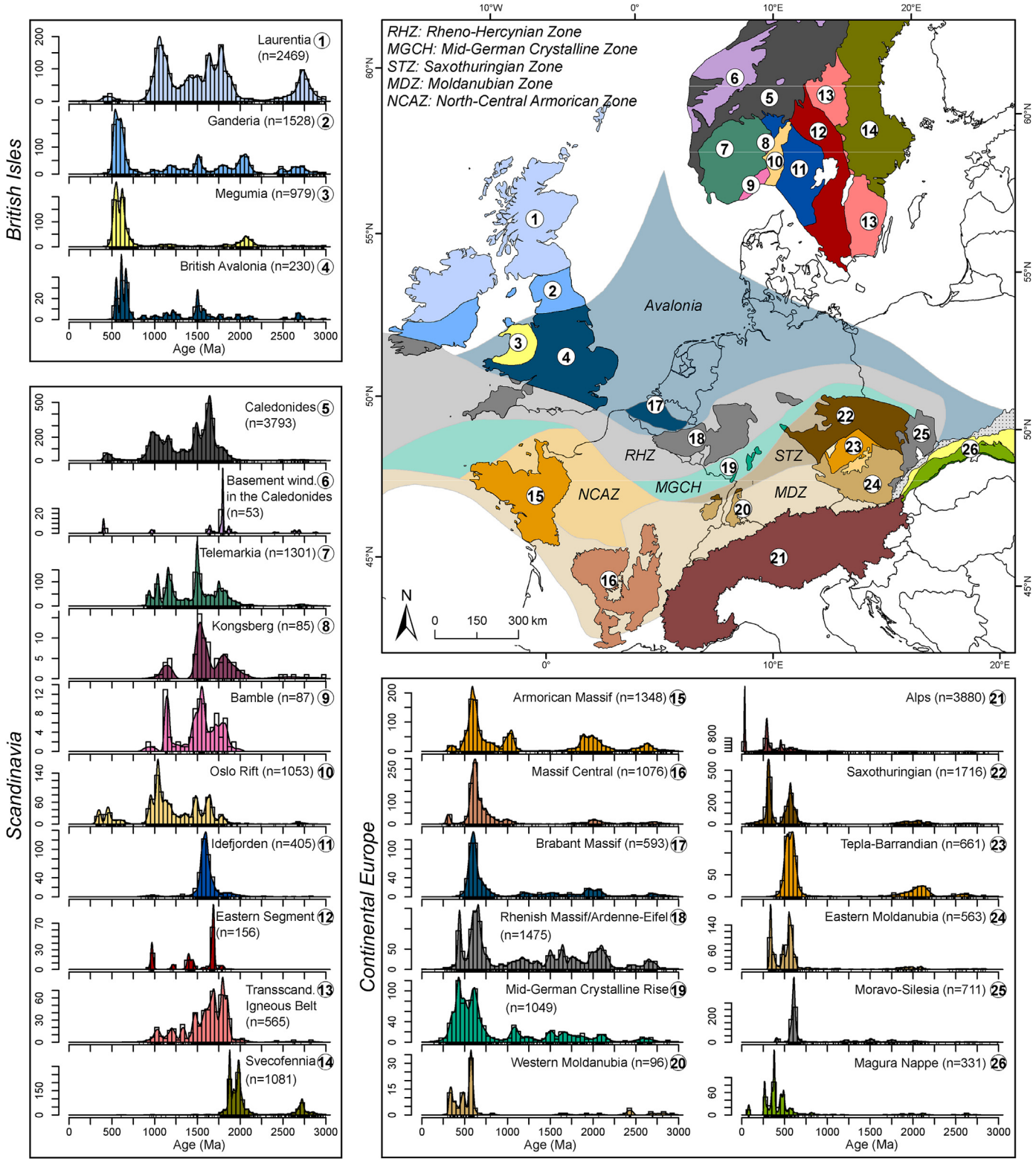

Fig. 7. KDE plots (adaptive bandwidth; Vermeesch, 2012) of published zircon ages from potential proto-source terranes (expanded after Bingen and Solli (2009), Fairey et al. (2018), Baykal et al. (2021), Bingen et al. (2021) and Stevens and Baykal (2021); see Appendix A for full references). Inset map shows simplified arrangement of potential source terranes (based on Verniers et al., 2008; Schmid et al., 2008; Ballèvre et al., 2009; Bingen and Solli, 2009; Babuška et al., 2010; Franke and Dulce, 2017; Fairey et al., 2018; Couzinié et al., 2019; Baykal et al., 2021; Bingen et al., 2021; Stevens and Baykal, 2021; other shapefiles used: P. Aureliano (PASC) 2020; thematicmapping.org).

zircon grains in fluvial sediments carried by the Rhine, which drains Peri-Gondwanan basement units (Fig. 4: RTe; Krippner and Bahlburg, 2013). Moreover, significant amounts of Variscan age zircon grains allowed inference of a mixed Peri-Gondwanan-Fennoscandian provenance for glaciofluvial sediments in the Northern European Plain (Fig. 4: SSS; Baykal et al., 2021).

Provenance studies of Palaeogene-Neogene sediments in the North Sea basin indicate derivation from multiple surrounding protosource regions. Detrital zircon U–Pb ages obtained from Miocene fluviodeltaic sands in the southeastern North Sea basin indicate derivation from a mixture of Fennoscandian terranes (Fig. 4: ENS; Olivarius et al., 2014). Shallow marine to estuarine sands of the Late Paleocene Thanet Fm. in the southwestern North Sea area are consistent with a mixed Avalonian-Laurentian source, likely derived from recycled Palaeozoic-Mesozoic sandstones in central Britain (Fig. 4: PBTF; Stevens and Baykal, 2021). Neogene marine/paralic sediments consist of recycled, mixed Peri-Gondwanan and northern Precambrian basement derived detritus, reinforcing the North Sea basin's history of extensive sediment reworking and mixing throughout the Cenozoic (Fig. 4: WNS; Verhaegen et al., 2021).

Detrital zircon U–Pb age analysis of the MIS 2 loess deposits from Pegwell Bay indicate temporal variability in protosource assemblages. The dominant Mesoproterozoic to Archean age zircon grain assemblage in the lower loess sample from Pegwell Bay (Fig. 4: PB210-230) is consistent with Precambrian protosource terranes in northern Britain and possibly Scandinavia. However, the late Palaeozoic Variscan age peak along with significant amounts of Late Neoproterozoic to Palaeozoic age zircon grains all suggest an additional contribution from Continental European protosources. By contrast, Peri-Gondwanan specific Variscan age grains are nearly absent in the upper loess sample (Fig. 4: PB130-150), while the minor proportions of Late Neoproterozoic to Palaeozoic age zircon grains as well as abundant Mesoproterozoic to Archean age grains are consistent with derivation entirely from British (and possibly Scandinavian) basement terranes. This protosource assessment is also reflected in the multi-dimensional scaling map (Fig. 8), where both Pegwell Bay loess samples plot fairly centrally between clusters of Precambrian basement terranes in northern Britain/Scandinavia and younger terranes in central-southern Britain/Continental Europe, with the deeper sample PB210-230 tending more towards the latter.

4.2. Late Quaternary sediment generation, dust emission sources, and transport pathways for loess in southeast Britain

Consideration of the possible protosource areas above allows some constraint over previously proposed sediment provenance and transport pathway scenarios for the loess at Pegwell Bay and southeast Britain. North Sea glaciofluvial sediments derived from the BIIS (Madgett and Catt, 1978; Bateman and Catt, 2007), the FIS (Eden, 1980) or proglacial lake Dogger account for the dominant Precambrian zircon age components in both Pegwell Bay loess samples (Fig. 4: SST, BT, 155VC). In addition, Variscan age zircon grains detected in the lower loess sample PB210-230 are consistent with partial derivation from fluvial sediments delivered to the

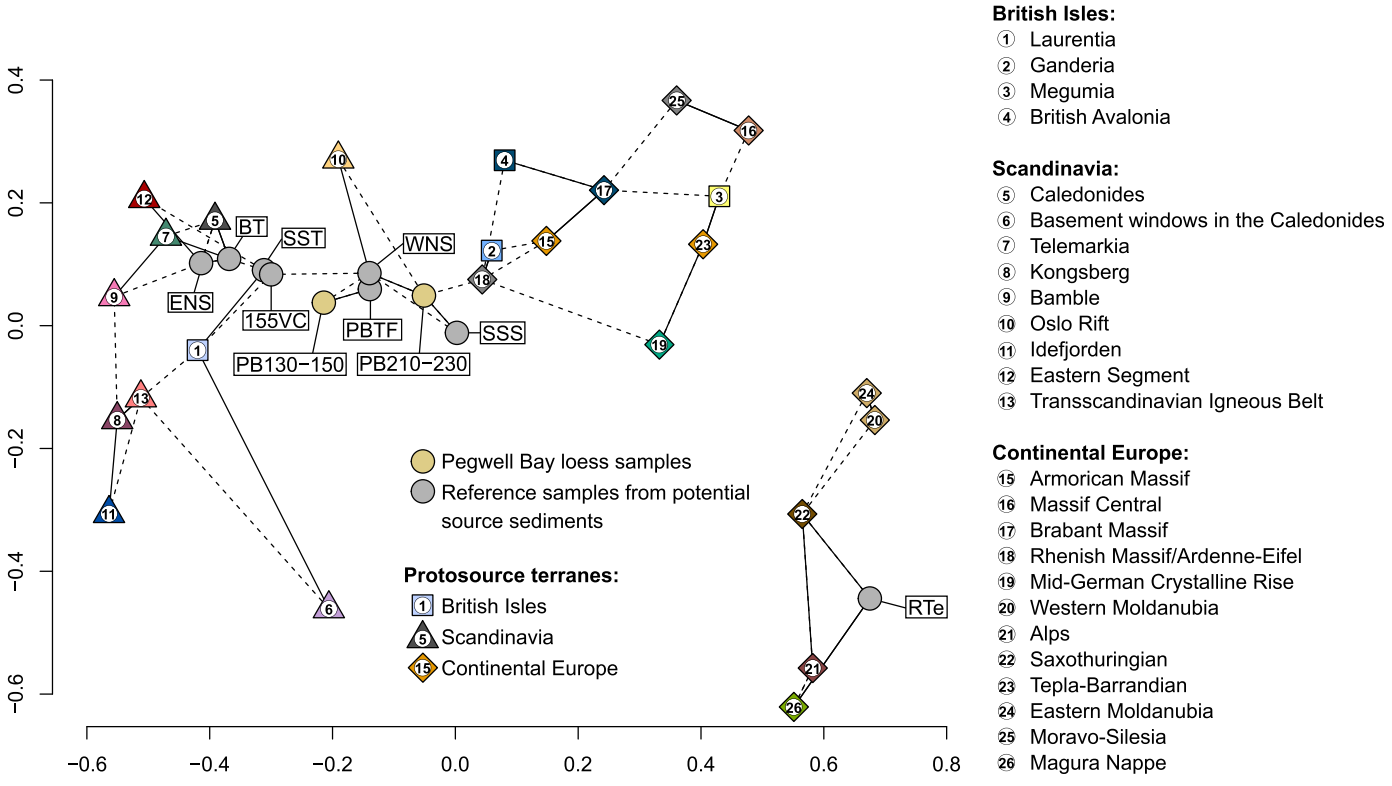

Fig. 8. Non-metric multi-dimensional scaling (MDS; Vermeesch, 2013) map using the Kolmogorov-Smirnov (KS) statistic for the zircon age data from loess at Pegwell Bay (PB130-150; PB210-230; this study), Palaeocene Thanet Fm. sands (PBTF; Stevens and Baykal, 2021), the LGM Skipsea Till (SST; this study); LGM Dogger lake sediment (155VC; this study), Neogene sediments in the southwestern North Sea basin (WNS; Verhaegen et al., 2021), Quaternary Rhine sediments (RTe; Krippner and Bahlburg, 2013), Late Pleistocene sandur sediments from the Northern European Plain (SSS; Baykal et al., 2021), the Late Pleistocene Black Till (BT; Knudsen et al., 2009) and Miocene deltaic sediments in the southeastern North Sea basin (ENS; Olivarius et al., 2014), alongside zircon age data compiled from potential protosource terranes (expanded after Bingen and Solli (2009), Fairey et al. (2018), Baykal et al. (2021), Bingen et al. (2021) and Stevens and Baykal (2021); see Appendix A for references; see Fig. 7 for simplified arrangement of potential protosource terranes). Svecofennia was excluded for ease of visualization, see Appendix A: Fig. 1 for MDS map including Svecofennia. Axes are dimensionless "K–S units" of the distance between samples. Solid and dashed lines connect samples with their closest and second closest neighbours, respectively.

North Sea region by rivers draining Continental Europe such as the previously proposed Rhine (Smalley et al., 2009; Krippner and Bahlburg, 2013), or via the FIS ice marginal spillway as reported from sandur sediments in the Northern European Plain (Baykal et al., 2021, Fig. 4: RTe, SSS).

However, loess provenance work using zircon geochronology alone may over represent proximal dust sources due to gravitational sorting during aeolian transport. In order to overcome this, we complement the zircon age framework with bulk Nd isotope data from loess at Pegwell Bay and potential source sediments across the North Sea region. Bulk Nd isotopic signatures of sediments are primarily controlled by the age of protosource rocks, with less radiogenic values representing older crustal sources (Goldstein and Jacobsen, 1987; Peucker-Ehrenbrink et al., 2010). The Nd isotopic composition of loess deposited at Pegwell Bay ranges from $\varepsilon Nd = -12.1$ to -13.1, with no significant trend over time or variation in accordance with dust deposition variability (dMAR) recorded at the site (Fig. 2). Grouped glacigenic samples from the FIS and BIIS margins yield relatively unradiogenic εNd values (FIS: -15.1; BIIS: -13.8) compared to more radiogenic values reported from Continental Europe derived fluvial sediments ($\varepsilon Nd = -11.0$; Fig. 2; Appendix A: Table 1), all consistent with the contrasting geological history of these terranes discussed in chapter 4.1.

While bulk Nd isotopic signatures of loess at Pegwell Bay are considerably less radiogenic than fluvial sediments carried by rivers draining Continental Europe, they are somewhat more radiogenic compared to the average signature of glacial detritus sampled along the BIIS or FIS margins (Fig. 2). This potentially indicates some constant input of younger Continental European crust-derived detritus to the loess. The fact that this signal is not recorded by zircon U–Pb ages from the upper loess sample, implies that this additional contribution from Continental European crust derived sediment may have been subject to gravitational sorting during longer range aeolian transport, and be concentrated more in the fine fraction of the loess (i.e., <10 μm). Alternatively, the Pegwell Bay loess Nd signature may imply sourcing from sediments of the late Palaeocene Thanet Fm underlying the loess, which yield an εNd value of -12.3 (Appendix A: Table 1), overlapping with the average composition of the loess. Indeed, detrital zircon ages reported from these shallow marine to estuarine sands of the late Palaeocene Thanet Fm (Stevens and Baykal, 2021), as well as Neogene marine/paralic sediments in the southwestern North Sea basin (Verhaegen et al., 2021), also resemble the zircon age distributions obtained from the loess, and thus cannot be excluded as potential dust sources to the loess based on crustal age source proxies alone (Fig. 4: PBTF & WNS). As such, crustal age information obtained from detrital zircon U–Pb age and bulk Nd isotope data alone may not be sufficient to discriminate between potential source sediments for loess in southeast England within the North Sea basin.

Analysis of heavy mineral assemblages and quartz grain morphology from loess and potential source sediments provides a means to further differentiate North Sea sediment sources to the loess. In contrast to ultrastable minerals such as zircon, other, less stable minerals are susceptible to weathering and dissolution during burial diagenesis (Morton and Hallsworth, 2007; Nie et al., 2013). Accordingly, mature sediments are enriched in the "most stable" heavy minerals also expressed by high ZTR maturity index values compared to bodies of more freshly eroded detritus. Amongst the studied sediments in the North Sea region (Fig. 5), shallow marine to fluviodeltaic sands of the late Palaeocene Thanet Fm. (PBTF) taken from directly underneath the Pegwell Bay loess predominantly consist of "most stable" minerals characterized by a high ZTR value (ZTR = 78), compared to much lower values reported from the loess at Pegwell Bay (PB140: 39.8; PB220: 36.6) or freshly eroded detritus deposited by last glacial ice sheets (BMT: 26, 155VC: 20) and the modern Rhine (MRW: 18.4). While Morton (1982) found that there was considerable variability in heavy mineral composition of the Thanet Fm. sands, less stable minerals were progressively lost towards the top of the formation, i.e., the part underlying the Quaternary loess. These upper Thanet Fm. sediments would be the most likely candidates for sourcing of the Quaternary loess at Pegwell Bay, yet the striking differences in heavy mineral composition make these sands unlikely as a major source for the overlying Pegwell Bay loess. Furthermore, SEM quartz grain analyses show that the two loess samples predominantly consist of angular to subangular grains, frequently exhibiting fracture marks specific to glacial grinding (Strand and Immonen, 2010; Mahaney, 2002, Fig. 6: A-H). These grain morphological observations indicate a substantial contribution of ice sheet derived sediments to the loess and lend further support for rejection of major sourcing from the late Palaeocene Thanet Fm., as well as other Miocene-Pliocene paralic/marine sediments in the southwestern North Sea basin, all deposited prior to the formation of extensive ice sheets in the Northern Hemisphere (Westerhold et al., 2020). Indeed, no such surface features are observed amongst rounded to subangular, often weathered grains from the Thanet Fm., consistent with the fluvial to shallow marine origin of these sediments (Mahaney, 2002, Fig. 6: I–K), affected by later Palaeogene acidic groundwater circulation (Morton, 1982).

The presence of glacially ground particles in the two loess samples indicated in the SEM analysis suggests dominant sourcing from BIIS and/or FIS derived glaciofluvial sediments. However, zircon age assemblages obtained from the respective till samples derived from these terranes are limited to Precambrian and Caledonian age grains, lacking the additional Variscan and/or Cadomian age grains detected in the two loess samples from Pegwell Bay (Fig. 4). Nevertheless, glacial till deposits are heterogeneous by definition and it is unclear how representative the reported till data are for wider BIIS and FIS derived detritus. In fact, Nd isotope signatures of glacigenic sediment samples collected along the BIIS and FIS margins exhibit substantial variability (Appendix A: Table 1). In particular, differences between the BIIS derived Skipsea Till and Basement Till are evident in Nd isotopic compositions (Appendix A: Table 1: SST: $\varepsilon Nd = -14.33$; BMT: $\varepsilon Nd = -15.12$) as well as heavy mineral spectra, suggesting this may also be the case for zircon age assemblages from these different till samples (Figs. 4 and 5). In particular, the heavy mineral spectrum obtained from the Skipsea Till is enriched in "most stable" minerals (ZTR = 57.3), implying this till may in fact be largely composed of glacially recycled ancient sandstone rather than fresh detritus eroded from Laurentian basement. Widespread cover sandstones across Britain are in turn derived from a range of protosources including Cadomian terranes in central-southern Britain (Avalonia), but also in part including material eroded from the active Variscan belt to the south (Morton et al., 2021). Glacial erosion of these differently sourced sandstones or Avalonian basement in central Britain would result in provenance variability amongst glaciofluvial sediments derived from the BIIS, which could potentially also include Variscan and/or Cadomian age zircon grains, as detected in the loess samples. As such, the provenance signature of both upper and lower loess at Pegwell Bay is reconcilable with sourcing from glacial detritus derived from the BIIS. Elevated ZTR values reported from the loess samples seem dominantly controlled by weathering of rather unstable pyroxene, causing enrichment of ultrastable minerals. In contrast, rapidly deposited glacial till sediments or subaequeous Dogger lake sediments are less affected by weathering, as indicated by larger contents of these unstable minerals. These postdepositional weathering effects may account for the differences in ZTR values

between loess and the glacigenic sediment samples, and thus do not contradict a glacially derived source to the loess at Pegwell Bay.

An alternative explanation for the origins of the Variscan to Cadomian age zircon grains detected in the lower loess sample may be sourcing from fluvial sediments derived from Continental Europe. Indeed, slight differences in quartz grain morphology were observed between the two Pegwell Bay loess samples, with relatively lower abundance of angular grains and less distinct glacial grinding related surface features reported from the lower loess sample PB210-230. This is somewhat consistent with findings from more quantitative grain morphological analyses of nearby loess exposed at Ospringe where a remarkable change from dominantly round-edged grains in the lower loess to dominantly sharp-edged grains in the upper loess was observed (Milodowski et al., 2015), reinforcing the potential for a non-glacial source contribution to the former. However, this temporal change in Pegwell Bay loess provenance recorded by zircon age assemblages and quartz grain morphology seems to contradict the consistent bulk εNd values obtained from the lower and upper loess units (Fig. 2). In particular, the mixture of fluvial sediments derived from Continental Europe and BIIS sources proposed for the lower loess sample PB210-230 would be expected to lead to a more radiogenic bulk Nd isotopic signature than for the upper loess sample PB130-150, purely derived from BIIS sources (Fig. 2). One possible explanation for the consistent εNd signatures reported from the two loess units may be additional sourcing from least radiogenic FIS derived sediments for the lower loess sample PB210-230, averaging out any additional input of more radiogenic detritus delivered by rivers draining Continental Europe and masking temporal protosource variability. Fluvial sediments carried by the Rhine are a potential candidate for the Continental Europe derived contribution detected in the lower loess sample. However, heavy mineral assemblage data from Rhine sediments exhibit notable differences to the composition of the loess (Fig. 5: MRW). In particular, the composition of the "most stable" mineral group is depleted in zircon and rutile but enriched in tourmaline compared to the composition of the loess. Moreover, the proportion of "less stable" hornblende is lower than in the Pegwell Bay loess. Given the presence of the "least stable" olivine in the Rhine sample but not in the loess, postdepositional reduction of hornblende can be excluded as factor in the differences between the Rhine and loess samples, and instead, these differences may reflect differences in detrital mineral assemblages, suggesting that the Rhine is not a source to the lower loess at Pegwell Bay. However, mixing of Rhine sediment with a more dominant glacially derived source in the North Sea basin could dilute these differences in heavy mineral spectra and further heavy mineral analyses of Rhine sediments are needed to test this fully. Nevertheless, a number of rivers draining central Continental Europe such as the Ems, Weser or Elbe potentially also transported Variscan derived grains into the North Sea basin, possibly accounting for the mixed lower loess provenance signature (Figs. 1 and 7). Moreover, mixed fluvial-glaciofluvial sediments transported via the FIS ice marginal spillway supplied readily mixed Peri-Gondwanan-Baltica-derived detritus to the North Sea region (Fig. 4: SSS), and would also be consistent with the possibility for Scandinavian-derived components in the lower loess.

Overall then, while the data presented here show that the upper loess sample at Pegwell Bay seems entirely BIIS derived, there are a number of possible explanations for the lower loess sample. BIIS contributions still dominate, and may explain the whole assemblage, but an additional contribution from mixed FIS and Central European sediments is also plausible, perhaps via glaciofluvial systems draining the FIS front on the Northern European Plain.

4.3. Sources through time

Detailed luminescence dating suggests two phases of greatly enhanced dust deposition centered on 25–23.5 ka and 20–19 ka at Pegwell Bay (Fig. 2; Stevens et al., 2020). The first of these dust accumulation phases coincides with Heinrich event 2 (Hemming, 2004), a particularly dusty period as recorded in dust archives around the Northern Hemisphere (Hovan et al., 1989; Rasmussen et al., 2014; Stevens et al., 2016; Újvári et al., 2017). Different atmospheric regimes have been proposed to account for this phase of enhanced dustiness over Europe (Antoine et al., 2009; Ludwig et al., 2016; Pinto and Ludwig, 2020). Regional climate-dust models suggest that the LGM dust cycle was dominantly controlled by east sector winds caused by the formation of a large-scale anticyclone over the coupled BIIS/FIS (36%) and southwards deflected cyclones (22%) (Schaffernicht et al., 2020). These winds would have provided ideal conditions for dust deflation from the exposed, proglacial North Sea basin and transport across Britain. However, while the coupling of the BIIS and FIS may have been essential for this atmospheric constellation over northern Europe, its role in controlling North Sea drainage may have been even more critical in driving episodic dust fall over NW Europe.

Crucially, ice sheet coalescence in the North Sea basin (28–26 ka; Roberts et al., 2018; Clark et al., 2022) redirected significant drainage of both BIIS and FIS derived meltwater southwestwards via the Channel, also incorporating river drainage from Continental Europe (Figs. 1 and 9 a)). However, glacioisostatic depression of the central North Sea facilitated formation of the ice-dammed lake Dogger along this proglacial drainage network (Roberts et al., 2018; Emery et al., 2019). The extent of this proglacial lake is uncertain, while its catchment potentially included drainage of the nearby coalesced BIIS and FIS as well as rivers draining Continental Europe likely deflected northwards by forebulge upwarping of the southern North Sea region (Fig. 1; Busschers et al., 2007). As such, Dogger lake sediment provenance is expected to vary spatially across the lake. Zircon U–Pb age and Nd isotope data of sediments from the western lake Dogger (155VC, Fig. 4, Appendix A: Table 1) indicate derivation from British basement while mixed Scandinavian-Continental European sediment provenance may be predicted to dominate in eastern parts of the lake (Figs. 1 and 9). During subsequent ice sheet retreat (25 ka; Fig. 9 b)), large parts of the eastern sector of the BIIS – here referred to as North Sea Lobe (NSL) – disintegrated and may have caused initial partial drainage of the Dogger lake (Roberts et al., 2018; Evans et al., 2021). Mixed glaciofluvial and lake sediments released during this event potentially included particles derived from protosources in Britain, Scandinavia and Continental Europe. Subsequently, braided river systems routed these sediments into the southern North Sea and the Channel, with floodplains acting as ready, nearby sources for dust deflation and accelerated loess build-up in southeast England (Figs. 2 and 9 b)). Sample PB210-230 from the lower loess at Pegwell Bay corresponds to the end of this first phase of accelerated loess deposition and indeed, the abundant mixed Variscan and Precambrian age zircon grains detected in this sample are consistent with sourcing from these mixed ice sheet derived and proglacial lake sediments. Additional input from reworked preexisting cover sediments in the North Sea basin (Rhine sediment, Palaeogene-Neogene sediment) is also possible, although a major source contribution from these deposits to the loess is excluded based on the provenance data, and inconsistent with the abrupt onset of loess accumulation at 25 ka.

During the following re-advance (22–21 ka; Fig. 9 c)), the NSL impinged on the north Norfolk coast while being restricted to the west of the Dogger bank moraine complex, the latter acting as

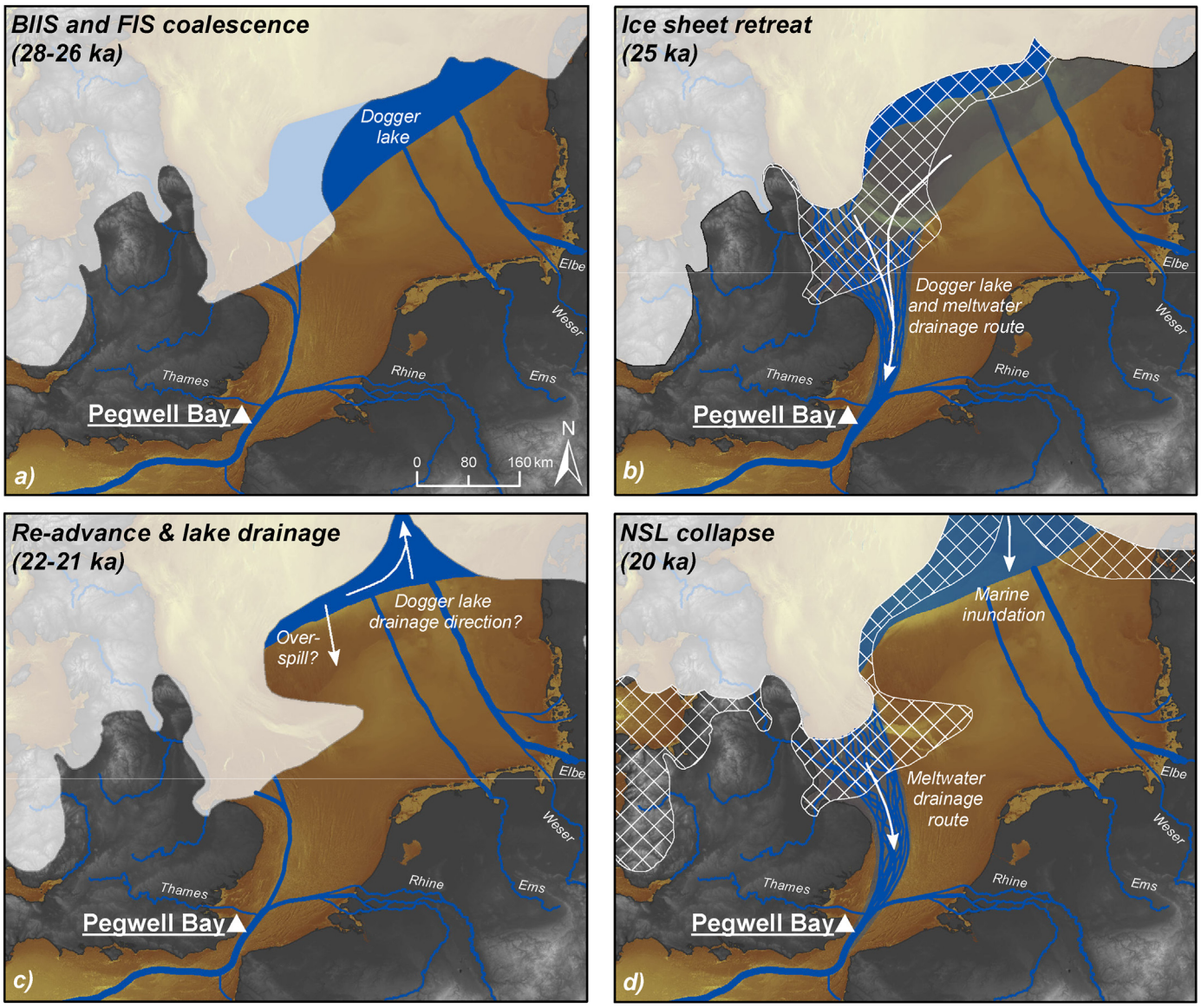

Fig. 9. Simplified model of ice sheet dynamics, associated proglacial drainage and Dogger lake evolution in the North Sea basin between 28 and 20 ka. Ice sheet margins and lake extents are based on Roberts et al. (2018), timing of ice sheet evolution is based on Clark et al. (2022): Fig. 5. See Fig. 1 for wider geographical context.

topographic barrier (Roberts et al., 2018; Evans et al., 2021; Clark et al., 2022). This NSL re-advance was likely triggered by the decoupling of the BIIS and FIS, which led to northerly drainage of lake Dogger (Roberts et al., 2018). However, the timing of this ice sheet unzipping in the North Sea is uncertain and Clark et al. (2022) infer an age of 21–20 ka, slightly postdating the previously proposed age by Roberts et al. (2018) (22–21 ka). The subsequent retreat of the NSL happened rapidly at c. 20 ka, as recorded in a series of recessional moraines on the western side of the North Sea basin (Fig. 9 d; Roberts et al., 2018; Evans et al., 2021; Clark et al., 2022). As for the previous retreat, considerable amounts of sediment laden glacial meltwater would have been released into the southern North Sea basin during this final NSL collapse, and routed towards the Channel. Both the timing of this NSL retreat and the new provenance data suggest that the resultant, sudden availability of BIIS derived sediment acted as source for the second phase of accelerated loess accumulation at Pegwell Bay (Fig. 2: 20–19 ka). The extreme fluvio-hydraulic transport energy of these glacial floodwaters is preserved in deeply incised streamlined channels along their drainage route (García-Moreno, 2017; De Clercq, 2018) as well as V-shaped percussion marks observed amongst quartz grains from the upper loess sample corresponding to this second accumulation phase (Mahaney, 2002; Wright, 2007, Fig. 6 D). The near absence of Variscan age zircon grains in this upper loess sample (PB130-150) may preclude a significant contribution from Dogger lake to this event of sediment supply, consistent with northerly drainage of the proglacial lake. In fact, Roberts et al. (2019) reported several radiocarbon ages from glacimarine sediments in the central North Sea, indicating marine inundation of this area by 19.9–19.5 ka. Due to the uncoupling of the BIIS and FIS, the semi-permanent anticyclone over northern Europe likely shifted eastwards and the influence of dust transport efficient east sector winds over the North Sea basin was reduced. In any case, remaining northeasterly-southeasterly winds were sufficient to account for enhanced dust transport to southeast England from the newly available close-by dust source (Stevens et al., 2020). As the NSL retreated, meltwater flow was later directed northwards preventing further supply of glaciofluvial sediment to the southern North

Sea, consistent with subsequent reduced dust accretion recorded at Pegwell Bay (Fig. 2).

According to this model, episodic loess deposition over southeast England is primarily a function of sediment availability in the southern North Sea, with strong east sector dust transport favoring winds likely augmenting peak deposition during the first accumulation phase. The complex interaction of dynamic NSL advance and retreat patterns with regional topography and drainage resulted in sudden events of high sediment supply and availability in the southern North Sea, driving loess deposition and provenance variability recorded at Pegwell Bay. This raises the possibility that the distribution and age of much of the loess distributed along the North Sea and English Channel may be a function of this ice sheet dynamics controlled drainage, and indeed that wider dust emission from NW Europe is also a function of these ice sheet processes. Notably, marine sediment cores from the Bay of Biscay at the western outlet of the Channel (Fig. 1) also record increased terrigenous sediment input (increased Fe/Ca and Ti/Ca ratios and increased turbidite flux) coincident with the two phases of enhanced loess deposition at Pegwell Bay (Fig. 2; Toucanne et al., 2015). Although Toucanne et al. (2015) dominantly attributed these meltwater pulses to FIS recession phases, this supports the suggestion that localized controls on sediment supply in the North Sea basin and subsequent drainage of sediment laden meltwater along the Channel may drive enhanced dust activity over a wider area of NW Europe and beyond. Testing the role of these meltwater pulses in driving wider scale dust emission and loess deposition requires further detailed chronological and provenance study of loess across the Channel region.

4.4. EIS contributions to wider MIS 2 dust activity and the role of ice sheets in coupled dust-climate events during the Quaternary

Based on identification of dominant BIIS and proglacial lake Dogger derived sources for loess at Pegwell Bay we demonstrate that ice sheet recession and associated increased sediment availability in the proglacial North Sea caused episodic dust fall over southeast England during the LGM and early deglaciation. However, greatly enhanced atmospheric dustiness during MIS 2 is recorded by peak loess accumulation more widely along the European loess belt (Guérin et al., 2017; Újvári et al., 2017; Zens et al., 2017; Perić et al., 2018; Moska et al., 2019; Fischer et al., 2021; Schmidt et al., 2021). Notably, Perić et al. (2022) show greatly enhanced MIS 2 (especially during Heinrich event 2) dust accumulation in a source distal loess site in Serbia, well away from potential local river floodplain sources, raising the question as to how much enhanced dust deposition in Europe may be attributed to ice sheet contributions.

The occurrence of glacial mega-floods during EIS recession phases is not restricted to the North Sea region. Instead, mega-flood specific landforms are also preserved throughout the Northern European Plain (Weckwerth et al., 2019), indicating that related events of sediment supply occurred more widely along the EIS margin during the early deglaciation. Indeed, previous research on loess provenance in the Northern European Plain detected substantial proportions of FIS derived material in the loess, mixed with approximately equal amounts of locally derived detritus (Baykal et al., 2021; Waroszewski et al., 2021). However, this mixed sediment provenance was detected in potential source sediments widespread across the region, resulting from long-term mixing through glacial and fluvial sediment reworking prior to deflation and loess deposition. As such, although ice sheet derived sediments contributed considerably to the thick last glacial loess deposits in the Northern European Plain, increased availability of these sources was excluded as cause of greatly enhanced MIS 2 dust deposition recorded in the studied loess (Baykal et al., 2021). Furthermore, while Smalley and Leach (1978) suggested that EIS meltwater floods may have carried northern ice sheet derived sediments through the Moravian depression in the Central European Highlands, acting as source for loess in the Carpathian basin, recent empirical loess provenance investigation refutes this (Buggle et al., 2008; Ujvári et al., 2012; Baykal et al., 2021; Fenn et al., 2022). Accordingly, northern ice sheet sediment supply is not the cause of accelerated loess accumulation in the Carpathian basin during MIS 2, although the dynamics of the Alpine Ice Sheet may have played a role (Bertran et al., 2021). Instead, fluctuations in dustiness during MIS 2 recorded in the region's loess deposits are argued to be modulated by large-scale North Atlantic climate reorganizations (Újvári et al., 2017).

As such, it seems likely that the greatly enhanced dustiness recorded by peak MIS 2 loess accumulation across Europe includes enhanced emission from a variety of sources. This implies that increased availability of glacially derived sediments during EIS recession may only have caused enhanced dust deposition in regions adjacent to proglacial drainage, as supported by increased MIS 2 loess accumulation across northern Europe, from the British Isles and Western France across the Northern European Plain (Guérin et al., 2017; Zens et al., 2017; Moska et al., 2019; Stevens et al., 2020). Although this region still represents an extensive area, it is one where loess is generally thinner and more intermittently found than in central and eastern Europe (Lehmkuhl et al., 2021). Taken at face value, this pattern of loess coverage potentially undermines the importance of ice sheets in dust production. However, one other important factor explaining this pattern may be the reduced preservation potential of dust deposits in or close to highly dynamic ice marginal regions. Here we argue that this apparently generally thinner, intermittent loess coverage should not be taken as indicative of reduced dust activity compared to central Europe. Instead, we argue that dust emission from ice sheet processes, particularly associated with abrupt meltwater events, are of considerable importance and impact.

Loess deposits in southeast England and along the Channel coasts are elevated compared to the North Sea/Channel basins, and thus protected from erosion through glacial meltwater floods channeled through these depressions, as well as subsequent post glacial sea level rise. In other regions marginal to the EIS, such as the Northern European Plain, meltwater drainage route is less predefined by topography and likely to vary through time causing extensive erosion of close-by loess deposits (Fig. 1). Loess provenance studies across the region agree that aeolian dust transport happens over rather short distances (Nawrocki et al., 2019; Pańczyk et al., 2020; Baykal et al., 2021). Accordingly, the lack of preserved loess in direct vicinity to the ice-marginal spillway in the Northern European Plain is likely due to subsequent erosion and taken at face value causes underrepresentation of glacially derived dust source contributions. In addition, long term mixing and ice sheet reworking of Fennoscandian and central European sediments in the ice marginal region of the Northern European Plain may mask the importance of ice sheet advances in driving enhanced loess accumulation and dust activity in provenance studies, as shown by the mixed Fennoscandian and mountainous continental European protosource assemblage of zircons in MIS 2 EIS sandur sediments in central Poland (Baykal et al., 2021). Furthermore, much more extensive loess likely existed in the now submerged North Sea and Channel basins (Lefort et al., 2019), and much of the preexisting loess in NW Europe in Britain and France is likely heavily reworked and eroded by slope, fluvial and periglacial processes (Catt, 1977; Bunce et al., 2022). Away from this highly dynamic ice marginal drainage environment, as well as the influence of central European mountains, loess accumulation on the Northern European Plain in

Ukraine and western Russia appears dominated by eastern EIS sediment contributions and the effect of ice sheet fluctuations (Nawrocki et al., 2019; Költringer et al., 2022). The extensive area of loess coverage in this region is testament to the wider role of ice sheets in dust production, and large river systems in dust distribution (Lehmkuhl et al., 2021; Költringer et al., 2022), further implying that reduced preservation of loess deposits in proglacial regions further west leads to underestimation of the influence of EIS derived dust sources.

By extension, this "preservation bias" may be misleading in terms of understanding the dominant causes of dust activity in Europe. Loess in southeast England (and along the English Channel generally) is unusual in that it is preserved exceptionally close to the drainage route of EIS derived meltwater. We propose that the record of dust activity in this loess caused by increased sediment availability in the proglacial zone may be widely representative for MIS 2 dust emission along the EIS margin. As demonstrated by the restricted time period of loess accumulation at Pegwell Bay (Stevens et al., 2020), the impact of this EIS-derived dust may be extensive but short lived, contingent on highly specific ice sheet configurations and interactions with regional topography. Dust-climate modelling should take this highly variable ice sheet contribution to wider dust loading into consideration if accurate estimates of past dust loading, emission and climate forcing are to be made. Furthermore, we argue that this model explains the close coupling of abrupt climate change events, EIS fluctuations and meltwater pulses, and enhanced dust accumulation, at least across NW Europe and the Northern European Plain. Abrupt EIS fluctuations and meltwater events not only affect ocean circulation and North Atlantic climate (Toucanne et al., 2015, 2021), they also simultaneously drive increased atmospheric dustiness over a wide area. Thus, we hypothesize that the observed abrupt climate, dust, and oceanographic events of the last glacial phase (Denton et al., 2010; Rasmussen et al., 2014; Lynch-Stieglitz, 2017; Újvári et al., 2017) are linked in northern Europe via the dynamics of continental ice sheets and their drainage events. This mechanism would reconcile the causes of abrupt changes in climate and dust activity in many areas during HE 2, and may in part explain the periodic occurrence of coupled dust and climate events widely seen in Quaternary dust records. However, we stress that these implications require testing through further targeted chronological and provenance study of loess deposits near proglacial drainage systems along the EIS margin, e.g. across the Channel but also east from the North Sea basin, and that in more ice sheet distal loess regions other processes will dominate loess accumulation.

Finally, fluctuations in the extent of the EIS not only interact with regional dust cycling through sediment supply to ice marginal regions. Past global climate model simulations indicate that the last glacial EIS was accompanied by a semi-permanent high-pressure system that influenced regional atmospheric circulation (COHMAP members, 1988; Ludwig et al., 2016). In particular, the coupling of the FIS and BIIS during the LGM caused formation of a large anticyclone that controlled dust transporting winds over Europe including dominant strong east sector winds over proglacial dust source regions (Schaffernicht et al., 2020). While our analysis of ice marginal loess deposits in southeast England shows that such enhanced dust transporting winds were not critical for near source loess deposition (see chapter 4.3), this atmospheric constellation may have promoted wider-scale atmospheric dispersal of ice sheet derived dust particles during the LGM. Indeed, chronologies from source distant loess deposits in central Europe also report enhanced dust accumulation rates during HE 2 (Perić et al., 2022) which opens up the possibility for ice sheet derived dust source contributions to enhanced atmospheric dust loading more widely. Moreover, high spatial resolution regional dust cycle simulations demonstrate that this anticyclonic circulation over the EIS may have facilitated dust transport from proglacial source regions in Europe as far as Greenland during the LGM, possibly contributing to peak dust particle concentrations in Greenland ice cores (Újvári et al., 2022). This scenario is consistent with multiple isotope source proxies that reveal overlapping signatures of European dust sources and dust particles recovered from LGM segments of the NGRIP ice core (Újvári et al., 2022). However, the issue of the sources of dust to Greenland during MIS 2 now requires extensive further investigation.

5. Conclusions

Coupled climate-dust events are recorded in Quaternary dust archives around the globe. Ice sheet fluctuations and meltwater pulses that affect ocean circulation are commonly considered as driver of these abrupt climatic changes. Furthermore, the release of large quantities of sediment rich meltwater and proglacial drainage turns ice marginal regions into efficient dust sources, potentially accounting for concurrent enhanced atmospheric dust loading. However, the role of ice sheets in generating sufficient source material to cause atmospheric dust loading more widely is debated. Loess deposits along the northern fringe of the European loess belt record accelerated dust deposition during MIS 2 when the Eurasian Ice Sheet was at its most dynamic. Nevertheless, uncertainties over the sources of this material limit understanding of the causes of this enhanced atmospheric dustiness. Extensive compilation of published and new sediment source proxy data from potential dust source sediments along the Eurasian Ice Sheet margin as well as basement terranes across Europe enables us to both discriminate between potential dust source signatures, but also retrace their protosources. Based on this framework we analyze the provenance of high sampling resolution luminescence dated late Quaternary loess deposits from southeast England, preserved exceptionally close to the drainage route of the last Eurasian Ice Sheet. Multi-proxy evidence reveals that ice sheet derived material dominated the sources to this ice marginal loess. Moreover, ice marginal dynamics in the North Sea caused sudden events of proglacial sediment supply, in turn driving atmospheric dust activity. Further review of MIS 2 dust provenance more widely highlights the potential for a substantial contribution from Eurasian Ice Sheet derived sources to greatly enhanced atmospheric dustiness over Europe and beyond. As such, we propose that in addition to driving changes in ocean circulation through meltwater pulses, ice sheet dynamics may also have driven abrupt changes in atmospheric dust activity. This mechanism would, at least in part, explain the coupling of dust and climate during short term climate events.

Author statement

TS, YB and MDB conceived and designed the study. TS, YB and MDB undertook fieldwork. KP conducted automated heavy mineral identification. AB and SŠ undertook SEM analyses of quartz grain morphology. HZ and JN undertook and oversaw Nd isotope measurements. YB compiled published zircon U–Pb data from Cenozoic sediments across the North Sea region and protosource terranes in Europe. YB, TS, AB and MDB undertook data interpretation. YB wrote the submission with help from TS, while all authors contributed to its revision and final version.

Declaration of competing interest

The authors declare that they have no known competing financial interests or personal relationships that could have appeared to influence the work reported in this paper.

Data availability

Data is available in supplementary files.

Acknowledgements

We are grateful to Ian Smalley and Pascal Bertran for their constructive reviews, which have significantly improved this manuscript. This work was funded by the Swedish Research Council (VR grant 2017–03888), the Quaternary Research Association (QRA) Quaternary Research Fund and the Anna Maria Lundin foundation. Sample VC155 was collected as part of the Natural Environment Research Council consortium grant; BRITICE-CHRONO NE/J009768/1 and thanks are extended to those who originally collected the core. Miriam Baykal and Ragna Orbe are thanked for their help during field work, and Thanet District Council is thanked for site access.

Appendix A. Supplementary data

Supplementary data to this article can be found online at https://doi.org/10.1016/j.quascirev.2022.107804.

References

Adebiyi, A.A., Kok, J.F., 2020. Climate models miss most of the coarse dust in the atmosphere. Sci. Adv. 6, 1–10. https://doi.org/10.1126/sciadv.aaz9507.

Antoine, P., Catt, J., Lautridou, J.P., Sommé, J., 2003. The loess and coversands of northern France and southern England. J. Quat. Sci. 18, 309–318. https://doi.org/10.1002/jqs.750.

Antoine, P., Rousseau, D.D., Moine, O., Kunesch, S., Hatté, C., Lang, A., Tissoux, H., Zöller, L., 2009. Rapid and cyclic aeolian deposition during the Last Glacial in European loess: a high-resolution record from Nussloch, Germany. Quat. Sci. Rev. 28, 2955–2973. https://doi.org/10.1016/j.quascirev.2009.08.001.

Babuška, V., Plomerová, J., Vecsey, L., 2010. Links between the structure of the mantle lithosphere and morphology of the cheb basin (eger rift, central Europe). Int. J. Earth Sci. 99, 1535–1544. https://doi.org/10.1007/s00531-010-0531-4.

Ballèvre, M., Bosse, V., Ducassou, C., Pitra, P., 2009. Palaeozoic history of the Armorican Massif: models for the tectonic evolution of the suture zones. Compt. Rendus Geosci. 341, 174–201. https://doi.org/10.1016/j.crte.2008.11.009.

Bao, Z., Zong, C., Fang, L., Yuan, H., Chen, K., Dai, M., 2018. Determination of Hf–Sr–Nd isotopic ratios by MC-ICP-MS using rapid acid digestion after flux-free fusion in geological materials. Acta Geochimica 37, 244–256. https://doi.org/10.1007/s11631-017-0207-x.

Bateman, R.M., Catt, J.A., 2007. Chapter 5 provenance and palaeoenvironmental interpretation of superficial deposits, with particular reference to post-depositional modification of heavy mineral assemblages. Dev. Sedimentol. 58, 151–188. https://doi.org/10.1016/S0070-4571(07)58005-2.

Bateman, M.D., Evans, D.J.A., Buckland, P.C., Connell, E.R., Friend, R.J., Hartmann, D., Moxon, H., Fairburn, W.A., Panagiotakopulu, E., Ashurst, R.A., 2015. Last glacial dynamics of the Vale of York and North Sea lobes of the British and Irish ice sheet. PGA (Proc. Geol. Assoc.) 126, 712–730. https://doi.org/10.1016/j.pgeola.2015.09.005.

Bateman, M.D., Evans, D.J.A., Roberts, D.H., Medialdea, A., Ely, J., Clark, C.D., 2018. The timing and consequences of the blockage of the Humber Gap by the last British–Irish Ice Sheet. Boreas 47, 41–61. https://doi.org/10.1111/bor.12256.

Baykal, Y., Stevens, T., Engström-Johansson, A., Skurzyński, J., Zhang, H., He, J., Lu, H., Adamiec, G., Költringer, C., Jary, Z., 2021. Detrital zircon U–Pb age analysis of last glacial loess sources and proglacial sediment dynamics in the Northern European Plain. Quat. Sci. Rev. 274. https://doi.org/10.1016/j.quascirev.2021.107265.

Bertran, P., Bosq, M., Borderie, Q., Coussot, C., Coutard, S., Deschodt, L., Franc, O., Gardère, P., Liard, M., Wuscher, P., 2021. Revised map of European aeolian deposits derived from soil texture data. Quat. Sci. Rev. 266. https://doi.org/10.1016/j.quascirev.2021.107085.

Bingen, B., Solli, A., 2009. Geochronology of magmatism in the Caledonian and Sveconorwegian belts of Baltica: synopsis for detrital zircon provenance studies. Norw. J. Geol. 89, 267–290.

Bingen, B., Viola, G., Möller, C., Auwera, J. Vander, Laurent, A., Yi, K., 2021. The Sveconorwegian orogeny. Gondwana Res. 90, 273–313. https://doi.org/10.1016/j.gr.2020.10.014.

Black, L.P., Kamo, S.L., Williams, I.S., Mundil, R., Davis, D.W., Korsch, R.J., Foudoulis, C., 2003. The application of SHRIMP to Phanerozoic geochronology; a critical appraisal of four zircon standards. Chem. Geol. 200, 171–188. https://doi.org/10.1016/S0009-2541(03)00166-9.

Black, L.P., Kamo, S.L., Allen, C.M., Davis, D.W., Aleinikoff, J.N., Valley, J.W., Mundil, R., Campbell, I.H., Korsch, R.J., Williams, I.S., Foudoulis, C., 2004. Improved 206Pb/238U microprobe geochronology by the monitoring of a trace-element-related matrix effect; SHRIMP, ID-TIMS, ELA-ICP-MS and oxygen isotope documentation for a series of zircon standards. Chem. Geol. 205, 115–140. https://doi.org/10.1016/j.chemgeo.2004.01.003.

Bogdanova, S.V., Bingen, B., Gorbatschev, R., Kheraskova, T.N., Kozlov, V.I., Puchkov, V.N., Volozh, Y.A., 2008. the East European craton (Baltica) before and during the assembly of Rodinia. Precambrian Res. 160, 23–45. https://doi.org/10.1016/j.precamres.2007.04.024.

Brendryen, J., Haflidason, H., Yokoyama, Y., Haaga, K.A., Hannisdal, B., 2020. Eurasian Ice Sheet collapse was a major source of Meltwater Pulse 1A 14,600 years ago. Nat. Geosci. 13, 363–368. https://doi.org/10.1038/s41561-020-0567-4.

Buggle, B., Glaser, B., Zöller, L., Hambach, U., Markovic, S., Glaser, I., Gerasimenko, N., 2008. Geochemical characterization and origin of Southeastern and Eastern European loesses (Serbia , Romania , Ukraine). Quat. Sci. Rev. 27, 1058–1075. https://doi.org/10.1016/j.quascirev.2008.01.018.

Bullard, J.E., Baddock, M., Bradwell, T., Crusius, J., Darlington, E., Gaiero, D., Gassó, S., Gisladottir, G., Hodgkins, R., McCulloch, R., McKenna-Neuman, C., Mockford, T., Stewart, H., Thorsteinsson, T., 2016. High-latitude dust in the Earth system. Rev. Geophys. 447–485. https://doi.org/10.1002/2016RG000518.

Bunce, C., Smalley, I., Stevens, T., Assadi-langroudi, A., 2022. Loess in Britain and Ireland : formation, modification and environmental significance , a review in memory of John Catt (1937 – 2017). PGA (Proc. Geol. Assoc.). https://doi.org/10.1016/j.pgeola.2022.06.005.

Busschers, F.S., Kasse, C., Balen, R.T. van, Vandenberghe, J., Cohen, K.M., Weerts, H.J.T., Wallinga, J., Johns, C., Cleveringa, P., Bunnik, F.P.M., 2007. Late Pleistocene evolution of the Rhine-Meuse system in the southern North Sea basin: imprints of climate change, sea-level oscillation and glacio-isostacy. Quat. Sci. Rev. 26, 3216–3248. https://doi.org/10.1016/j.quascirev.2007.07.013.

Catt, J.A., 1977. Loess and coversands. In: Shotton, F.W. (Ed.), In British Quaternary Studies: Recent Advances. Clarendon Press. Oxford 222–229.

Catt, J.A., Staines, S.J., 1982. Loess in cornwall. Proc. Ussher Soc. 5, 368–375.

Catt, J.A., Bateman, R.M., Wintle, A.G., Murphy, C.P., 1987. The loess' section at borden, kent, SE England. J. Quat. Sci. 2, 141–147. https://doi.org/10.1002/jqs.3390020207.

Clark, C.D., Ely, J.C., Hindmarsh, R.C.A., Bradley, S., Eczi, A.I.G.N., Chiverrell, R.C., Scourse, J., Benetti, S., Bradwell, T.O.M., Burke, M., Callard, S.L., Medialdea, A., Saher, M., Small, D., Smedley, R.K., Gasson, E., Gregoire, L., Gandy, N., Ballantyne, C., Bateman, M.D., Bigg, G.R., Doole, J., Hughes, A.L.C., Moreton, S., Pollard, D., Praeg, D., Sejrup, H.P., Mccarron, S., Landeghem KJJ, V.A.N., Wilson, P., Bateman, M.D., Grant, R., Clark, C.D., Ely, J.C., Bradley, S., Ign, A., 2022. Growth and retreat of the last British – Irish Ice Sheet , 31 000 to 15 000 years ago : the BRITICE-CHRONO reconstruction. Boreas. https://doi.org/10.1111/bor.12594.

Clercq, M. De, 2018. Drowned Landscapes of the Belgian Continental Shelf. PhD Dissertation. Gent University, Belgium.

Couzinié, S., Laurent, O., Chelle-Michou, C., Bouilhol, P., Paquette, J.L., Gannoun, A.M., Moyen, J.F., 2019. Detrital zircon U–Pb–Hf systematics of Ediacaran metasediments from the French Massif Central: consequences for the crustal evolution of the north Gondwana margin. Precambrian Res. 324, 269–284. https://doi.org/10.1016/j.precamres.2019.01.016.

Denton, G.H., Anderson, R.F., Toggweiler, J.R., Edwards, R.L., Schaefer, J.M., Putnam, A.E., 2010. The last glacial termination. Science 328, 1652–1656. https://doi.org/10.1126/science.1184119.

Eden, D.N., 1980. The loess of north-east essex, England. Boreas 9, 165–177. https://doi.org/10.1111/j.1502-3885.1980.tb01039.x.

Emery, A.R., Hodgson, D.M., Barlow, N.L.M., Carrivick, J.L., Cotterill, C.J., Phillips, E., 2019. Left high and dry: deglaciation of Dogger bank, North Sea, recorded in proglacial lake evolution. Front. Earth Sci. 7, 1–27. https://doi.org/10.3389/feart.2019.00234.

Evans, D.J.A., Roberts, D.H., Bateman, M.D., Clark, C.D., Medialdea, A., Callard, L., Grimoldi, E., Chiverrell, R.C., Ely, J., Dove, D., Ó Cofaigh, C., Saher, M., Bradwell, T., Moreton, S.G., Fabel, D., Bradley, S.L., 2021. Retreat dynamics of the eastern sector of the British–Irish Ice Sheet during the last glaciation. J. Quat. Sci. 36, 723–751. https://doi.org/10.1002/jqs.3275.

Fairey, B.J., Kerrison, A., Meere, P.A., Mulchrone, K.F., Hofmann, M., Gärtner, A., Sonntag, B.L., Linnemann, U., Kuiper, K.F., Ennis, M., Mark, C., Cogné, N., Chew, D., 2018. Erratum: the provenance of the devonian old red sandstone of the dingle peninsula, SW Ireland; the earliest record of laurentian and peri-gondwanan sediment mixing in Ireland. In: Journal of the Geological Society, vol. 175. Journal of the Geological Society, London, p. 1032. https://doi.org/10.1144/jgs2017-099Err (2018) 175, (411-424), 10.1144/jgs20.

Fall, D.A., 2003. The Geotechnical and Geochemical Characterisation of the Brick-earth of Southern England. University of Portsmouth. Unpublished PhD dissertation.

Fenn, K., Millar, I.L., Durcan, J.A., Thomas, D.S.G., Banak, A., Marković, S.B., Veres, D., Stevens, T., 2022. The provenance of Danubian loess. Earth Sci. Rev. 226. https://doi.org/10.1016/j.earscirev.2022.103920.

Fischer, P., Jöris, O., Fitzsimmons, K.E., Vinnepand, M., Prud'homme, C., Schulte, P., Hatté, C., Hambach, U., Lindauer, S., Zeeden, C., Peric, Z., Lehmkuhl, F., Wunderlich, T., Wilken, D., Schirmer, W., Vött, A., 2021. Millennial-scale terrestrial ecosystem responses to upper pleistocene climatic changes: 4D-reconstruction of the schwalbenberg loess-palaeosol-sequence (middle rhine valley, Germany). Catena 196, 104913. https://doi.org/10.1016/j.catena.2020.104913.

Franke, W., Dulce, J.C., 2017. Back to sender: tectonic accretion and recycling of Baltica-derived Devonian clastic sediments in the Rheno-Hercynian Variscides. Int. J. Earth Sci. 106, 377–386. https://doi.org/10.1007/s00531-016-1408-y.
Freslon, Nicolas, Bayon, Germain, Toucanne, Samuel, Bermell, Sylvain, Bollinger, Claire, Cheron, Sandrine, Etoubleau, Joel, Germain, Yoan, Khripounoff, Alexis, Ponzevera, Emmanuel, Rouget, Marie-Laure, 2014. Rare earth elements and neodymium isotopes in sedimentary organic matter. Geochem. Cosmochim. Acta 140, 177–198. https://doi.org/10.1016/j.gca.2014.05.016.
Fuhrer, K., Wolff, E.W., Johnsen, S.J., 1999. Timescales for dust variability in the Greenland Ice Core Project (GRIP) ice core in the last 100,000 years. J. Geophys. Res. Atmos. 104, 31043–31052. https://doi.org/10.1029/1999JD900929.
García-Moreno, D., 2017. Origin and Geomorphology of Dover Strait and Southern North Sea Palaeovalleys and Palaeodepressions. Gent University, Belgium. Unpublished PhD dissertation.
Gehrels, G., Pecha, M., 2014. Detrital zircon U-Pb geochronology and Hf isotope geochemistry of Paleozoic and Triassic passive margin strata of western North America. Geosphere 10, 49–65. https://doi.org/10.1130/GES00889.1.
Gehrels, G., Valencia, V., Pullen, A., 2006. Detrital zircon geochronology by laser-ablation multicollector ICPMS at the Arizona laserchron center. Paleontological Society Papers. In: Geochronology: Emerging Opportunities, vol. 11. Paleontological Society Short Course, Philadelphia, PA, pp. 67–76. https://doi.org/10.1002/9781444347166.ch2. October 21, 2006.
Gehrels, G.E., Valencia, V.A., Ruiz, J., 2008. Enhanced precision, accuracy, efficiency, and spatial resolution of U-Pb ages by laser ablation-multicollector-inductively coupled plasma-mass spectrometry. G-cubed 9, 1–13. https://doi.org/10.1029/2007GC001805.
Goldstein, S.J., Jacobsen, S.B., 1987. The Nd and Sr isotopic systematics of river-water dissolved material: implications for the sources of Nd and Sr in seawater. Chem. Geol. Isot. Geosci. 66, 245–272.
Guérin, G., Antoine, P., Schmidt, E., Goval, E., Hérisson, D., Jamet, G., Reyss, J.L., Shao, Q., Philippe, A., Vibet, M.A., Bahain, J.J., 2017. Chronology of the Upper Pleistocene loess sequence of Havrincourt (France) and associated Palaeolithic occupations: a Bayesian approach from pedostratigraphy, OSL, radiocarbon, TL and ESR/U-series data. Quat. Geochronol. 42, 15–30. https://doi.org/10.1016/j.quageo.2017.07.001.
Hemming, S.R., 2004. Heinrich events: massive late Pleistocene detritus layers of the North Atlantic and their global climate imprint. Rev. Geophys. 42. https://doi.org/10.1029/2003RG000128.
Hovan, S.A., Rea, D.K., Pisias, N.G., Shackleton, N.J., 1989. A direct link between the China loess and marine δ18O records: aeolian flux to the north Pacific. Nature 340, 296–298.
Hughes, A.L.C., Gyllencreutz, R., Lohne, Ø.S., Mangerud, J., Svendsen, J.I., 2016. The last Eurasian ice sheets - a chronological database and time-slice reconstruction, DATED-1. Boreas 45, 1–45. https://doi.org/10.1111/bor.12142.
Jacobsen, S.B., Wasserburg, G.J., 1980. Sm-Nd isotopic evolution of chondrites. Earth Planet Sci. Lett. 50, 139–155. https://doi.org/10.1016/0012-821X(80)90125-9.
Jochum, K.P., Weis, U., Schwager, B., Stoll, B., Wilson, S.A., Haug, G.H., Andreae, M.O., Enzweiler, J., 2016. Reference values following ISO guidelines for frequently requested rock reference materials. Geostand. Geoanal. Res. 40, 333–350. https://doi.org/10.1111/j.1751-908X.2015.00392.x.
Kirkland, C.L., Daly, J.S., Whitehouse, M.J., 2007. Provenance and terrane evolution of the kalak nappe complex, Norwegian Caledonides: implications for neoproterozoic paleogeography and tectonics. J. Geol. 115, 21–41. https://doi.org/10.1086/509247.
Knippertz, P., 2014. Mineral Dust. https://doi.org/10.1007/978-94-017-8978-3.
Knudsen, C., Kokfelt, T., Aagaard, T., Bartholdy, J., Pejrup, M., 2009. Fingerprinting sediments along the west coast of Jylland: interpreting provenance data. Geol. Surv. Den. Greenl. Bull. 25–28. https://doi.org/10.34194/geusb.v17.5006.
Költringer, C., Stevens, T., Lindner, M., Baykal, Y., Ghafarpour, A., Khormali, F., Taratunina, N., Kurbanov, R., 2022. Quaternary sediment sources and loess transport pathways in the Black Sea - caspian Sea region identified by detrital zircon U-Pb geochronology. Global Planet. Change 209. https://doi.org/10.1016/j.gloplacha.2022.103736.
Koster, E.A., 2005. Recent advances in luminescence dating of Late Pleistocene (Cold-Climate) aeolian sand and loess deposits in western Europe. Permafr. Periglac. Process. 16, 131–143. https://doi.org/10.1002/ppp.512.
Krippner, A., Bahlburg, H., 2013. Provenance of Pleistocene Rhine River Middle Terrace sands between the Swiss–German border and Cologne based on U–Pb detrital zircon ages. Int. J. Earth Sci. 917–932. https://doi.org/10.1007/s00531-012-0842-8.
Lefort, J.P., Monnier, J.L., Danukalova, G., 2019. Transport of late pleistocene loess particles by katabatic winds during the lowstands of the English channel. J. Geol. Soc. 176, 1169–1181. https://doi.org/10.1144/jgs2019-070.
Lehmkuhl, F., Zens, J., Krauß, L., Schulte, P., Kels, H., 2016. Loess-paleosol sequences at the northern European loess belt in Germany: distribution, geomorphology and stratigraphy. Quat. Sci. Rev. 153, 11–30. https://doi.org/10.1016/j.quascirev.2016.10.008.
Lehmkuhl, F., Nett, J.J., Pötter, S., Schulte, P., Sprafke, T., Jary, Z., Antoine, P., Wacha, L., Wolf, D., Zerboni, A., Hošek, J., Marković, S.B., Obreht, I., Sümegi, P., Veres, D., Zeeden, C., Boemke, B., Schaubert, V., Viehweger, J., Hambach, U., 2021. Loess landscapes of Europe – mapping, geomorphology, and zonal differentiation. Earth Sci. Rev. 215, 103496. https://doi.org/10.1016/j.earscirev.2020.103496.
Li, Z.X., Bogdanova, S.V., Collins, A.S., Davidson, A., Waele, B. De, Ernst, R.E., Fitzsimons, I.C.W., Fuck, R.A., Gladkochub, D.P., Jacobs, J., Karlstrom, K.E., Lu, S., Natapov, L.M., Pease, V., Pisarevsky, S.A., Thrane, K., Vernikovsky, V., 2008. Assembly, configuration, and break-up history of Rodinia: a synthesis. Precambrian Res. 160, 179–210. https://doi.org/10.1016/j.precamres.2007.04.021.
Lill, G.O., Smalley, I.J., 1978. Distribution of loess in Britain. PGA (Proc. Geol. Assoc.) 89, 57–65. https://doi.org/10.1016/S0016-7878(78)80021-2.
Linnemann, U., Pereira, M.F., Jeffries, T.E., Drost, K., Gerdes, A., 2008. The cadomian orogeny and the opening of the rheic ocean: the diacrony of geotectonic processes constrained by LA-ICP-MS U-Pb zircon dating (Ossa-Morena and saxo-thuringian zones, iberian and bohemian massifs). Tectonophysics 461, 21–43. https://doi.org/10.1016/j.tecto.2008.05.002.
Ludwig, P., Schaffernicht, E.J., Shao, Y., Pinto, J.G., 2016. Regional atmospheric circulation over Europe during the last Glacial maximum and its links to precipitation. J. Geophys. Res. 121, 2130–2145. https://doi.org/10.1002/2015JD024444.
Lynch-Stieglitz, J., 2017. The atlantic meridional overturning circulation and abrupt climate change. Ann. Rev. Mar. Sci 1–22. https://doi.org/10.1146/annurev-marine-010816-060415.
Madgett, P.A., Catt, J.A., 1978. Petrography, stratigraphy and weathering of late pleistocene tills in east Yorkshire, lincolnshire and north Norfolk. Proc. Yorks. Geol. Soc. 42, 55–108.
Mahaney, W.C., 1995. Glacial crushing, weathering and diagenetic histories of quartz grains inferred from scanning electron microscopy. In: Menzies, J. (Ed.), Modern Glacial Environments - Processes. Dynamics and Sediments. Butterworth-Heinemann Ltd, Oxford, pp. 487–506.
Mahaney, W.C., 2002. Atlas of Sand Grain Surface Textures and Applications. Oxford University Press, p. 237.
Makishima, A., Nath, B.N., Nakamura, E., 2008. New sequential separation procedure for Sr, Nd and Pb isotope ratio measurement in geological material using MC-ICP-MS and TIMS. Geochem. J. 42, 237–246. https://doi.org/10.2343/geochemj.42.237.
Marren, P.M., 2002. Fluvial-lacustrine interaction on Skeioarărsandur, Iceland: implications for sandur evolution. Sediment. Geol. 149, 43–58. https://doi.org/10.1016/S0037-0738(01)00243-3.
McKerrow, W.S., Niocaill, C. Mac, Dewey, J.F., 2000. The caledonian orogeny redefined. J. Geol. Soc. 157, 1149–1154. https://doi.org/10.1144/jgs.157.6.1149.
Meinander, O., Dagsson-waldhauserova, P., Amosov, P., Aseyeva, E., Atkins, C., 2022. Newly identified climatically and environmentally significant high-latitude dust sources. Atmos. Chem. Phys. 11889–11930.
COHMAP members, 1988. Climatic changes of the last 18,000 Years: observations and model simulations. Science 241.
Milodowski, A.E., Northmore, K.J., Kemp, S.J., Entwisle, D.C., Gunn, D.A., Jackson, P.D., Boardman, D.I., Zoumpakis, A., Rogers, C.D.F., Dixon, N., Jefferson, I., Smalley, I.J., Clarke, M., 2015. The mineralogy and fabric of 'Brickearths' in Kent, UK and their relationship to engineering behaviour. Bull. Eng. Geol. Environ. 74, 1187–1211. https://doi.org/10.1007/s10064-014-0694-5.
Moine, O., Antoine, P., Hatté, C., Landais, A., Mathieu, J., Prud'homme, C., Rousseau, D.-D., 2017. The impact of Last Glacial climate variability in west-European loess revealed by radiocarbon dating of fossil earthworm granules. Proc. Natl. Acad. Sci. USA 114, 6209–6214. https://doi.org/10.1073/pnas.1614751114.
Morton, A.C., 1982. The provenance and diagenesis of Palaeogene sandstones of southeast England as indicated by heavy mineral analysis. PGA (Proc. Geol. Assoc.) 93, 263–274. https://doi.org/10.1016/S0016-7878(82)80003-5.
Morton, A.C., Hallsworth, C., 2007. Chapter 7 stability of detrital heavy minerals during burial diagenesis. Dev. Sedimentol. 58, 215–245. https://doi.org/10.1016/S0070-4571(07)58007-6.
Morton, A.C., Chisholm, J.I., Frei, D., 2021. Provenance of Carboniferous sandstones in the central and southern parts of the Pennine Basin, UK: evidence from detrital zircon ages. Proc. Yorks. Geol. Soc. 63. https://doi.org/10.1144/pygs2020-010.
Moska, P., Jary, Z., Adamiec, G., Bluszcz, A., 2019. Chronostratigraphy of a loess-palaeosol sequence in Biały Kościół Poland using OSL and radiocarbon dating. Quat. Int. 502, 4–17. https://doi.org/10.1016/j.quaint.2018.05.024.
Nawrocki, J., Bogucki, A.B., Gozhik, P., Łanczont, M., Pańczyk, M., Standzikowski, K., Komar, M., Rosowiecka, O., Tomeniuk, O., 2019. Fluctuations of the Fennoscandian Ice Sheet recorded in the anisotropy of magnetic susceptibility of periglacial loess from Ukraine. Boreas 48, 940–952. https://doi.org/10.1111/bor.12400.
Neace, E.R., Nance, R.D., Murphy, J.B., Lancaster, P.J., Shail, R.K., 2016. Zircon LA-ICPMS geochronology of the cornubian batholith, SW England. Tectonophysics 681, 332–352. https://doi.org/10.1016/j.tecto.2016.04.002.
Nie, J., Peng, W., Pfaff, K., Möller, A., Garzanti, E., Andò, S., Stevens, T., Bird, A., Chang, H., Song, Y., Liu, S., Ji, S., 2013. Controlling factors on heavy mineral assemblages in Chinese loess and red clay. Palaeogeogr. Palaeoclimatol. Palaeoecol. 381–382, 110–118. https://doi.org/10.1016/j.palaeo.2013.04.020.
Nie, J., Pullen, A., Garzione, C.N., Peng, W., Wang, Z., 2018. Pre-Quaternary decoupling between Asian aridification and high dust accumulation rates. Sci. Adv. 4. https://doi.org/10.1126/sciadv.aao6977.
Olivarius, M., Rasmussen, E.S., Siersma, V., Knudsen, C., Kokfelt, T.F., Keulen, N., 2014. Provenance signal variations caused by facies and tectonics : zircon age and heavy mineral evidence from Miocene sand in the north-eastern North Sea Basin. Mar. Petrol. Geol. 49, 1–14. https://doi.org/10.1016/j.marpetgeo.2013.09.010.
Pańczyk, M., Nawrocki, J., Bogucki, A.B., Gozhik, P., Łanczont, M., 2020. Possible

sources and transport pathways of loess deposited in Poland and Ukraine from detrital zircon U-Pb age spectra. Aeolian Res. 45. https://doi.org/10.1016/j.aeolia.2020.100598.
Patton, H., Hubbard, A., Andreassen, K., Auriac, A., Whitehouse, P.L., Stroeven, A.P., Shackleton, C., Winsborrow, M., Heyman, J., Hall, A.M., 2017. Deglaciation of the Eurasian ice sheet complex. Quat. Sci. Rev. 169, 148–172. https://doi.org/10.1016/j.quascirev.2017.05.019.
Perić, Z., Lagerbäck Adolphi, E., Stevens, T., Újvári, G., Zeeden, C., Buylaert, J.P., Marković, S.B., Hambach, U., Fischer, P., Schmidt, C., Schulte, P., Huayu, L., Shuangwen, Y., Lehmkuhl, F., Obreht, I., Veres, D., Thiel, C., Frechen, M., Jain, M., Vött, A., Zöller, L., Gavrilov, M.B., 2018. Quartz OSL dating of late quaternary Chinese and Serbian loess: a cross Eurasian comparison of dust mass accumulation rates. Quat. Int. 1–15. https://doi.org/10.1016/j.quaint.2018.01.010.
Perić, Z.M., Stevens, T., Obreht, I., Hambach, U., Lehmkuhl, F., Marković, S.B., 2022. Detailed luminescence dating of dust mass accumulation rates over the last two glacial-interglacial cycles from the Irig loess- palaeosol sequence, Carpathian Basin. Global Planet. Change 141267. https://doi.org/10.1016/j.gloplacha.2022.103895.
Perrin, R.M.S., Davies, H., Fysh, M.D., 1974. Distribution of late Pleistocene aeolian deposits in eastern and southern England. Nature 248, 320–324. https://doi.org/10.1038/248320a0.
Peucker-Ehrenbrink, B., Miller, M.W., Arsouze, T., Jeandel, C., 2010. Continental bedrock and riverine fluxes of strontium and neodymium isotopes to the oceans. G-cubed 11, 1–22. https://doi.org/10.1029/2009GC002869.
Pinto, J.G., Ludwig, P., 2020. Extratropical cyclones over the north atlantic and western Europe during the last glacial maximum and implications for proxy interpretation. Clim. Past 16, 611–626. https://doi.org/10.5194/cp-16-611-2020.
Pitcher, W.S., Shearman, D.J., Pugh, D.C., 1954. The loess of Pegwell Bay, kent, and its associated frost soils. Geol. Mag. 308–315.
Pullen, A., Ibáñez-Mejía, M., Gehrels, G.E., Ibáñez-Mejía, J.C., Pecha, M., 2014. What happens when n= 1000? Creating large-n geochronological datasets with LA-ICP-MS for geologic investigations. J. Anal. At. Spectrom. 29, 971–980. https://doi.org/10.1039/c4ja00024b.
Pullen, A., Ibáñez-Mejia, M., Gehrels, G.E., Giesler, D., Pecha, M., 2018. Optimization of a laser ablation-single collector-inductively coupled plasma-mass spectrometer (Thermo element 2) for accurate, precise, and efficient zircon U-Th-Pb geochronology. G-cubed 19, 3689–3705. https://doi.org/10.1029/2018GC007889.
Rahmstorf, S., 2002. Ocean circulation and climate during the past 120,000 years. Nature 419, 207–214. https://doi.org/10.1038/nature01090.
Rasmussen, S.O., Bigler, M., Blockley, S.P., Blunier, T., Buchardt, S.L., Clausen, H.B., Cvijanovic, I., Dahl-Jensen, D., Johnsen, S.J., Fischer, H., Gkinis, V., Guillevic, M., Hoek, W.Z., Lowe, J.J., Pedro, J.B., Popp, T., Seierstad, I.K., Steffensen, J.P., Svensson, A.M., Vallelonga, P., Vinther, B.M., Walker, M.J.C., Wheatley, J.J., Winstrup, M., 2014. A stratigraphic framework for abrupt climatic changes during the Last Glacial period based on three synchronized Greenland ice-core records: refining and extending the INTIMATE event stratigraphy. Quat. Sci. Rev. 106, 14–28. https://doi.org/10.1016/j.quascirev.2014.09.007.
Roberts, D.H., Evans, D.J.A., Callard, S.L., Clark, C.D., Bateman, M.D., Medialdea, A., Dove, D., Cotterill, C.J., Saher, M., Cofaigh, C., Chiverrell, R.C., Moreton, S.G., Fabel, D., Bradwell, T., 2018. Ice marginal dynamics of the last British-Irish ice sheet in the southern North sea: ice limits, timing and the influence of the Dogger bank. Quat. Sci. Rev. 198, 181–207. https://doi.org/10.1016/j.quascirev.2018.08.010.
Roberts, D.H., Grimoldi, E., Callard, L., Evans, D.J.A., Clark, C.D., Stewart, H.A., Dove, D., Saher, M., Ó Cofaigh, C., Chiverrell, R.C., Bateman, M.D., Moreton, S.G., Bradwell, T., Fabel, D., Medialdea, A., 2019. The mixed-bed glacial landform imprint of the North Sea Lobe in the western North Sea. Earth Surf. Process. Landforms 44, 1233–1258. https://doi.org/10.1002/esp.4569.
Rodushkin, I., Axelsson, M.D., Burman, E., 2000. Multielement analysis of coal by ICP techniques using solution nebulization and laser ablation. Talanta 51, 743–759. https://doi.org/10.1016/S0039-9140(99)00333-1.
Ruddiman, W.F., Molfino, B., Esmay, A., Pokras, E., 1980. Evidence bearing on the mechanism of rapid deglaciation. Climatic Change 3, 65–87. https://doi.org/10.1007/BF02423169.
Schaffernicht, E.J., Ludwig, P., Shao, Y., 2020. Linkage between dust cycle and loess of the last glacial maximum in Europe. Atmos. Chem. Phys. Discuss. 1–27. https://doi.org/10.5194/acp-2019-693.
Schmid, S.M., Bernoulli, D., Fügenschuh, B., Matenco, L., Schefer, S., Schuster, R., Tischler, M., Ustaszewski, K., 2008. The Alpine-Carpathian-Dinaridic orogenic system: correlation and evolution of tectonic units. Swiss J. Geosci. 101, 139–183. https://doi.org/10.1007/s00015-008-1247-3.
Schmidt, C., Zeeden, C., Krauß, L., Lehmkuhl, F., Zöller, L., 2021. A chronological and palaeoenvironmental re-evaluation of two loess-palaeosol records in the northern Harz foreland, Germany, based on innovative modelling tools. Boreas. https://doi.org/10.1111/bor.12510.
Scourse, J., Saher, M., Landeghem KJJ, . Van, Lockhart, E., Purcell, C., Callard, L., Roseby, Z., Allinson, B., Pieńkowski, A.J., O'Cofaigh, C., Praeg, D., Ward, S., Chiverrell, R., Moreton, S., Fabel, D., Clark, C.D., 2019. Advance and retreat of the marine-terminating Irish Sea ice stream into the celtic sea during the last glacial: timing and maximum extent. Mar. Geol. 412, 53–68. https://doi.org/10.1016/j.margeo.2019.03.003.
Sejrup, H.P., Clark, C.D., Hjelstuen, B.O., 2016. Rapid ice sheet retreat triggered by ice stream debuttressing: evidence from the North Sea. Geology 44, 355–358. https://doi.org/10.1130/G37652.1.
Sima, A., Kageyama, M., Rousseau, D.D., Ramstein, G., Balkanski, Y., Antoine, P., Hatté, C., 2013. Modeling dust emission response to North Atlantic millennial-scale climate variations from the perspective of East European MIS 3 loess deposits. Clim. Past 9, 1385–1402. https://doi.org/10.5194/cp-9-1385-2013.
Smalley, I.J., Leach, J.A., 1978. The origin and distribution of the loess in the Danube basin and associated regions of East-Central Europe - a review. Sediment. Geol. 21, 1–26. https://doi.org/10.1016/0037-0738(78)90031-3.
Smalley, I., Hara-dhand, K.O., Wint, J., Machalett, B., Jary, Z., Jefferson, I., 2009. Rivers and loess : the significance of long river transportation in the complex event-sequence approach to loess deposit formation. Quat. Int. 198, 7–18. https://doi.org/10.1016/j.quaint.2008.06.009.
Smedley, R.K., Scourse, J.D., Small, D., Hiemstra, J.F., Duller, G.A.T., Bateman, M.D., Burke, M.J., Chiverrell, R.C., Clark, C.D., Davies, S.M., Fabel, D., Gheorghiu, D.M., McCarroll, D., Medialdea, A., Xu, S., 2017. New age constraints for the limit of the British–Irish ice sheet on the Isles of scilly. J. Quat. Sci. 32, 48–62. https://doi.org/10.1002/jqs.2922.
Soulet, G., Ménot, G., Bayon, G., Rostek, F., Ponzevera, E., Toucanne, S., Lericolais, G., Bard, E., 2013. Abrupt drainage cycles of the fennoscandian ice sheet. Proc. Natl. Acad. Sci. U. S. A 110, 6682–6687. https://doi.org/10.1073/pnas.1214676110.
Stephan, T., Kroner, U., Romer, R.L., Rösel, D., 2019. From a bipartite Gondwanan shelf to an arcuate Variscan belt: the early Paleozoic evolution of northern Peri-Gondwana. Earth Sci. Rev. 192, 491–512. https://doi.org/10.1016/j.earscirev.2019.03.012.
Stevens, T., Baykal, Y., 2021. Detrital zircon U-Pb ages and source of the late Palaeocene Thanet Formation, kent, SE England. PGA (Proc. Geol. Assoc.) 132, 240–248. https://doi.org/10.1016/j.pgeola.2021.01.003.
Stevens, T., Lu, H., Thomas, D.S.G., Armitage, S.J., 2008. Optical dating of abrupt shifts in the late Pleistocene East Asian monsoon. Geology 36, 415–418. https://doi.org/10.1130/G24524A.1.
Stevens, T., Marković, S.B., Zech, M., Hambach, U., Sümegi, P., 2011. Dust deposition and climate in the Carpathian Basin over an independently dated last glacial-interglacial cycle. Quat. Sci. Rev. 30, 662–681. https://doi.org/10.1016/j.quascirev.2010.12.011.
Stevens, T., Carter, A., Watson, T.P., Vermeesch, P., Andò, S., Bird, A.F., Lu, H., Garzanti, E., Cottam, M.A., Sevastjanova, I., 2013. Genetic linkage between the yellow river, the mu us desert and the Chinese loess plateau. Quat. Sci. Rev. 78, 355–368. https://doi.org/10.1016/j.quascirev.2012.11.032.
Stevens, T., Buylaert, J.P., Lu, H., Thiel, C., Murray, A., Frechen, M., Yi, S., Zeng, L., 2016. Mass accumulation rate and monsoon records from Xifeng, Chinese Loess Plateau, based on a luminescence age model. J. Quat. Sci. 31, 391–405. https://doi.org/10.1002/jqs.2848.
Stevens, T., Sechi, D., Bradák, B., Orbe, R., Baykal, Y., Cossu, G., Tziavaras, C., Andreucci, S., Pascucci, V., 2020. Abrupt last glacial dust fall over southeast England associated with dynamics of the British-Irish ice sheet. Quat. Sci. Rev. 250. https://doi.org/10.1016/j.quascirev.2020.106641.
Strand, K., Immonen, N., 2010. Dynamics of the Barents-Kara ice sheet as revealed by quartz sand grain microtextures of the late Pleistocene Arctic Ocean sediments. Quat. Sci. Rev. 29, 3583–3589. https://doi.org/10.1016/j.quascirev.2010.09.017.
Strand, K., Passchier, S., Näsi, J., 2003. Implications of quartz grain microtextures for onset eocene/oligocene glaciation in prydz Bay, ODP site 1166, Antarctica. Palaeogeogr. Palaeoclimatol. Palaeoecol. 198, 101–111. https://doi.org/10.1016/S0031-0182(03)00396-1.
Tanaka, T., Togashi, S., Kamioka, H., Amakawa, H., Kagami, H., Hamamoto, T., Yuhara, M., Orihashi, Y., Yoneda, S., Shimizu, H., Kunimaru, T., Takahashi, K., Yanagi, T., Nakano, T., Fujimaki, H., Shinjo, R., Asahara, Y., Tanimizu, M., Dragusanu, C., 2000. JNdi-1: a neodymium isotopic reference in consistency with LaJolla neodymium. Chem. Geol. 168, 279–281. https://doi.org/10.1016/S0009-2541(00)00198-4.
Toucanne, S., Soulet, G., Freslon, N., Silva Jacinto, R., Dennielou, B., Zaragosi, S., Eynaud, F., Bourillet, J.F., Bayon, G., 2015. Millennial-scale fluctuations of the European Ice Sheet at the end of the last glacial, and their potential impact on global climate. Quat. Sci. Rev. 123, 113–133. https://doi.org/10.1016/j.quascirev.2015.06.010.
Toucanne, S., Soulet, G., Vázquez Riveiros, N., Boswell, S.M., Dennielou, B., Waelbroeck, C., Bayon, G., Mojtahid, M., Bosq, M., Sabine, M., Zaragosi, S., Bourillet, J.F., Mercier, H., 2021. the North atlantic glacial eastern boundary current as a Key driver for ice-sheet—AMOC interactions and climate instability. Paleoceanogr. Paleoclimatol. 36. https://doi.org/10.1029/2020PA004068.
Ujvári, G., Varga, A., Ramos, F.C., Kovács, J., Németh, T., Stevens, T., 2012. Evaluating the use of clay mineralogy, Sr-Nd isotopes and zircon U-Pb ages in tracking dust provenance: an example from loess of the Carpathian Basin. Chem. Geol. 304 (305), 83–96. https://doi.org/10.1016/j.chemgeo.2012.02.007.
Újvári, G., Stevens, T., Svensson, A., Klötzli, U.S., Manning, C., Németh, T., Kovács, J., Sweeney, M.R., Gocke, M., Wiesenberg, G.L.B., Markovic, S.B., Zech, M., 2015. Two possible source regions for central Greenland last glacial dust. Geophys. Res. Lett. 42, 10399–10408. https://doi.org/10.1002/2015GL066153.
Újvári, G., Stevens, T., Molnár, M., Demény, A., Lambert, F., Varga, G., Jull, A.J.T., Páll-Gergely, B., Buylaert, J.-P., Kovács, J., 2017. Coupled European and Greenland last glacial dust activity driven by North Atlantic climate. Proc. Natl. Acad. Sci. USA 201712651. https://doi.org/10.1073/pnas.1712651114.
Toucanne, S., Zaragosi, S., Bourillet, J.-F., Dennielou, B., Jorry, S.J., Jouet, G., Cremer, M., 2012. External controls on turbidite sedimentation on the glacially-influenced Armorican margin (Bay of Biscay, western European margin). Mar. Geol. 303-306, 137–153. https://doi.org/10.1016/j.margeo.2012.02.008.

Újvári, G., Klötzli, U., Stevens, T., Svensson, A., Ludwig, P., Vennemann, T., Gier, S., Horschinegg, M., Palcsu, L., Hippler, M., Kovacs, J., Biagio, C. Di, Formenti, P., 2022. Greenland ice core record of last glacial dust sources and atmospheric circulation. J. Geophys. Res. Atmos. https://doi.org/10.1029/2022JD036597.

Vandenberghe, J., Woo, M.K., 2002. Modern and ancient periglacial river types. Prog. Phys. Geogr. 26, 479–506. https://doi.org/10.1191/0309133302pp349ra.

Verhaegen, J., Eynatten, H. Von, Dunkl, I., Weltje, G.J., 2021. Detrital zircon geochronology and heavy mineral analysis as complementary provenance tools in the presence of extensive weathering, reworking and recycling: the Neogene of the southern North Sea Basin. Geol. Mag. 158, 1572–1584. https://doi.org/10.1017/S0016756821000133.

Vermeesch, P., 2004. How many grains are needed for a provenance study? Earth Planet Sci. Lett. 224, 441–451. https://doi.org/10.1016/j.epsl.2004.05.037.

Vermeesch, P., 2012. On the visualisation of detrital age distributions. Chem. Geol. 312–313, 190–194. https://doi.org/10.1016/j.chemgeo.2012.04.021.

Vermeesch, P., 2013. Multi-sample comparison of detrital age distributions. Chem. Geol. 341, 140–146. https://doi.org/10.1016/j.chemgeo.2013.01.010.

Verniers, J., Maletz, J., Kriz, J., Zigaite, Z., Paris, F., Schönlaub, H.P., Wrona, R., 2008. Silurian. Geological Society London Special Publications.

Wang, C.Y., Campbell, I.H., Stepanov, A.S., Allen, C.M., Burtsev, I.N., 2011. Growth rate of the preserved continental crust: II. Constraints from Hf and O isotopes in detrital zircons from Greater Russian Rivers. Geochem. Cosmochim. Acta 75, 1308–1345. https://doi.org/10.1016/j.gca.2010.12.010.

Waroszewski, J., Pietranik, A., Sprafke, T., Kabała, C., Frechen, M., Jary, Z., Kot, A., Tsukamoto, S., Meyer-Heintze, S., Krawczyk, M., Łabaz, B., Schultz, B., Erban Kochergina, Y.V., 2021. Provenance and paleoenvironmental context of the Late Pleistocene thin aeolian silt mantles in south-west Poland – a widespread parent material for soils. Catena 204. https://doi.org/10.1016/j.catena.2021.105377.

Weckwerth, P., Wysota, W., Piotrowski, J.A., Adamczyk, A., Krawiec, A., Dąbrowski, M., 2019. Late Weichselian glacier outburst floods in North-Eastern Poland: landform evidence and palaeohydraulic significance. Earth Sci. Rev. 194, 216–233. https://doi.org/10.1016/j.earscirev.2019.05.006.

Westerhold, T., Marwan, N., Drury, A.J., Liebrand, D., Agnini, C., Anagnostou, E., Barnet, J.S.K., Bohaty, S.M., Vleeschouwer, D. De, Florindo, F., Frederichs, T., Hodell, D.A., Holbourn, A.E., Kroon, D., Lauretano, V., Littler, K., Lourens, L.J., Lyle, M., Pälike, H., Röhl, U., Tian, J., Wilkens, R.H., Wilson, P.A., Zachos, J.C., 2020. An astronomically dated record of Earth's climate and its predictability over the last 66 million years. Science 369, 1383–1388. https://doi.org/10.1126/SCIENCE.ABA6853.

Wright, J.S., 2007. An overview of the role of weathering in the production of quartz silt. Sediment. Geol. 202, 337–351. https://doi.org/10.1016/j.sedgeo.2007.03.024.

Zens, J., Schulte, P., Klasen, N., Krauß, L., Pirson, S., Burow, C., Brill, D., Eckmeier, E., Kels, H., Zeeden, C., Spagna, P., Lehmkuhl, F., 2017. OSL chronologies of paleo-environmental dynamics recorded by loess-paleosol sequences from Europe: case studies from the Rhine-Meuse area and the Neckar Basin. Palaeogeogr. Palaeoclimatol. Palaeoecol. https://doi.org/10.1016/j.palaeo.2017.07.019.

Zhang, H., Nie, J., Liu, X., Pullen, A., Li, G., Peng, W., Zhang, H., 2021. Spatially variable provenance of the Chinese loess plateau. Geology 49, 1155–1159. https://doi.org/10.1130/G48867.1.